Journal of Magnetic Resonance **151,** 9–27 (2001)
doi:10.1006/jmre.2001.2326, available online at http://www.idealibrary.com on IDEAL®

Modeling Magnetization Transfer Using a Three-Pool Model and Physically Meaningful Constraints on the Fitting Parameters

Toni Ceckler,[1] James Maneval, and Brian Melkowits[2]

Department of Chemistry and Department of Chemical Engineering, Bucknell University, Lewisburg, Pennsylvania 17837

Received March 22, 2000; revised November 7, 2000; published online May 18, 2001

A model for water–macromolecular magnetization transfer is presented which addresses the mechanism of coupling between the hydrogen populations and the extraction of physically meaningful parameters from experimental magnetization transfer data. Both physical exchange between bulk-solvent and site-specific hydration-layer hydrogens and *inter*molecular magnetic dipolar coupling between these specific hydration-layer-solvent and macromolecular hydrogens are explicitly included, leading to a three-pool model for magnetization transfer. It is shown that the three-pool model is well approximated by a two-pool model for coupling between the bulk-solvent and macromolecular hydrogens when the dipolar-coupled solvent hydrogens are a small fraction of the total solvent, and the solvent–macromolecular coupling constant includes both dipolar magnetic, κ_{dip}, and physical exchange, κ_{ex}, coupling rates. The model is also extended to multiple solvent systems. The model results in a set of coupled equations that predict magnetization transfer spectra as a function of temperature and composition. Physically meaningful constraints on the coupling and relaxation parameters are established for systems in which magnetization transfer has been observed including solvated cross-linked proteins and lipid bilayers. Using parameter estimates based on these constraints, empirical magnetization transfer spectra are well predicted by the model. It is found that the degree of magnetization transfer becomes independent of κ_{dip} and κ_{ex} when these parameters become greater than about 50 s^{-1}. In the semi-rigid cross-linked protein systems where the mobility of the macromolecular matrix is insensitive to temperature, the magnitude of the observed magnetization transfer is consistent with being limited by the intermolecular dipolar coupling and spin–lattice relaxation in the bulk-solvent phase.

Key Words: **magnetization transfer; three-pool model; constraining fitting parameters.**

INTRODUCTION

The interactions of water at macromolecular surfaces play a critical role in the functional properties of hydrated macromolecular systems (*1–12*). It is these same interactions which can be exploited using water as a probe of hydrated macromolecular systems, such as in MRI (*13*). These heterogeneous systems can be described as complex matrices of macromolecules with water filling the space created by the supramolecular structure. A layer of water will be associated with the surface of the macromolecular matrix. The properties, dynamics, and structure of the water in the solvation layer are coupled to and therefore contain information about the macromolecular physicochemistry. Exchange mixes the water populations such that, on the time scale of the exchange, the observable bulk-water properties are a weighted average of the properties of the separate regions. Characterizing these interactions is important in being able to exploit bulk-water properties as a probe of structure and properties of the macromolecular matrix and in gaining a fundamental understanding of the behavior and structure of water in hydrated systems.

Water hydrogen NMR is useful in characterizing hydrated systems due to the sensitivity of nuclear magnetic relaxation to water–macromolecular interactions and the timescales of the dynamics governing those interactions (*4, 5, 8, 9, 14–16*). Magnetization is coupled within the ^{1}H populations through mechanisms which exchange nuclear magnetizations of the bulk-water, macromolecular, and hydration-layer populations, including (1) through-space nuclear magnetic dipolar interactions between macromolecular hydrogens and specific hydration-layer waters and/or labile waters within the macromolecular structure and (2) physical exchange of hydrogens between these specific sites and the bulk-water phase; see Fig. 1 (*17–20*). Physical exchange may include both molecular exchange and water–macromolecular exchange of labile hydrogens. Magnetic dipole–dipole coupling results in the through-space transfer of magnetization (*21*). Physical exchange mixes the coupling site and bulk-water hydrogen populations. Through magnetic dipole–dipole coupling and exchange, the water hydrogen NMR is coupled to the dynamic, conformational, and structural properties of the hydrated macromolecular system. Although the general theory describing water–macromolecular hydrogen nuclear coupling has been known since the late 1970s (*16, 22–24*), the physicochemistry and dynamics governing the contribution of each process to the observable effects in the bulk-water phase are not well characterized. This is in part a result of the complexity of the coupled interactions, the resulting mathematical description, and the difficulty in separating and determining the

[1] To whom correspondence should be addressed. E-mail: caraidgh@together.net.

[2] Current address: Department of Chemistry, University of Georgia, Athens, GA 30602-2556.

1090-7807/01 $35.00

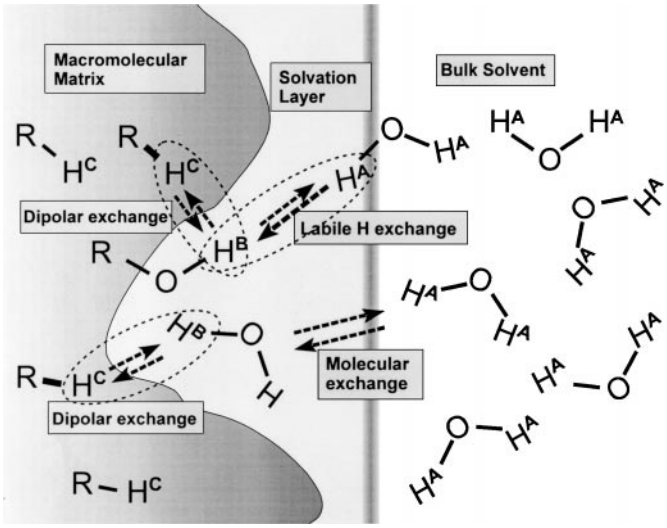

FIG. 1. Schematic of proton populations and magnetization transfer exchange pathways in hydrated macromolecular systems. A, Bulk-solvent hydrogens; B, solvent hydrogens dipolar coupled to macromolecular hydrogens; C, macromolecular hydrogens.

magnitudes of the parameters on which the bulk-water NMR signal depends.

Coupling between hydrogen populations can be exploited experimentally to characterize interactions within the system using the technique of magnetization transfer (*25, 26*). In the presence of magnetic dipolar coupling at the macromolecular surface, selective saturation of the nuclear magnetization of the macromolecular hydrogen population results in a decrease in the nuclear magnetization of the directly coupled water hydrogens through the nuclear Overhauser effect (*16, 21*). This effect will be referred to here as dipolar transfer. The rate and steady-state magnitude of dipolar transfer are directly related to the strength of dipolar coupling which will depend on the physicochemistry of the coupling site on the macromolecular surface (*17, 27*). The slower the relative motion and the smaller the separation of the coupled hydrogens in the site, the greater the dipolar coupling strength, resulting in a faster rate of transfer and greater decrease in the steady-state magnetization of the directly coupled water hydrogens. The decrease of the surface-water magnetization due to dipolar transfer is transferred to the bulk-water phase through physical exchange. The overall process of dipolar transfer and physical exchange leading to a decrease in the observable bulk-water NMR signal in the presence of saturation of the macromolecular magnetization is what will be referred to in the present work as magnetization transfer (MT). The degree of magnetization transfer has been found to be specific to the type of hydrated system (*5, 8, 17, 28, 29*). In human tissue, a significant magnetization transfer effect has been observed in muscle, the lens and cornea of the eye, cartilage, and gray and white matter of the brain (*30*). This suggests that the degree of magnetization transfer may be used as a characteristic parameter of the system and is currently being exploited to enhance MRI contrast (*30–32*).

Convincing evidence that both dipolar coupling and physical exchange play a significant role in magnetization transfer has been demonstrated in hydrated systems of lipid bilayers, proteins, and gels (*5, 7, 8, 16, 17, 19, 20, 28, 33–36*). Work with hydrated lipids suggests that magnetic coupling occurs at specific dynamically restricted sites on the hydrophilic bilayer surface which are also characterized by the apparent necessity for the presence of a hydrogen-donor functionality such as a hydroxyl, amine, or carboxyl group (*17, 19, 27, 36, 37*). The role the hydrogen donor plays in coupling the water and macromolecular hydrogen populations has not been unambiguously established. It may serve as a site for hydrogen exchange of labile solvent and macromolecular hydrogens, with dipolar coupling between these labile hydrogens and the bulk of the macromolecular hydrogen population. Another possibility is that the hydrogen donor acts as a hydrogen bonding site to orient the solvent molecules at the macromolecular surface, allowing for dipolar coupling directly between the solvent and macromolecular hydrogens (*17, 19, 28, 35, 36*). Magnetization transfer has been observed using solvents without exchangeable hydrogens, suggesting that hydrogen exchange at these hydrogen-donor groups is not a necessary requirement for magnetization transfer (*28*). Initial work studying the pH dependence of magnetization transfer suggested that hydrogen exchange played some role in coupling the water and macromolecular populations (*27, 36*). Further work suggests that the observable pH dependence of magnetization transfer is due to structural changes in the macromolecular system leading to changes in the magnitude of dipolar coupling (*19*). This evidence supports the idea that the role of the hydrogen-donor functional groups is to serve as anchors to hold solvent molecules on or within the macromolecular matrix.

Several quantitative models have been proposed to account for magnetization transfer. The simplest models identify only the bulk solvent and macromolecular hydrogen populations with coupling described by a single coupling constant (*5, 16, 17, 28, 38, 39, 40*). These models are inherently incomplete where both physical exchange and dipolar coupling lead to magnetization transfer. With two coupling processes there are, at the least, three distinct coupled hydrogen populations which include the macromolecular hydrogens, solvent hydrogens in the macromolecular dipolar coupling site, and hydrogens in the bulk-solvent phase. The coupling processes are mechanistically different and described by two distinct coupling constants. Some recent work has addressed the limitations of using a two-pool model by the *ad hoc* introduction of a coupling constant which combines both physical exchange and dipolar coupling into an effective coupling constant (*19, 28*).

Multipool models have been presented to describe magnetization transfer (*5, 18–20, 34, 41*) where both physical exchange and dipolar coupling are explicitly included. Most of this work addresses magnetization transfer qualitatively and/or under limiting conditions of complete saturation of macromolecular

magnetization (*34*) or of relative rates of physical and dipolar exchange (*5, 19*).

In this work a quantitative model for magnetization transfer is presented, starting with a three-pool model incorporating both physical exchange and dipolar coupling using the Bloch equation formalism. It is shown that there are reasonable conditions under which the three-pool model reduces to a bulk-solvent and macromolecular hydrogen two-pool model with an appropriately defined coupling constant which includes rate constants for both dipolar coupling and physical exchange. A goal here is to use the three-pool model to derive a set of equations describing the steady-state magnetizations which are then used to model empirical MT data starting with reasonable limits for the parameters included in the coupled rate equations. Temperature is an important variable which will be used to assess which relaxation process may limit the observable degree of magnetization transfer since the variation of the observable MT with temperature must be consistent with the temperature dependence of the limiting processes (*42*). This approach to modeling MT results in the assessment of how each relaxation pathway may effect the bulk-solvent signal intensity, places constraints on the parameters, and can be used to assess the validity of values extracted from fitting empirical MT data using analytical solutions to the coupled rate equations.

THEORY

The formulation of the coupled rate equations used to describe the transfer of nuclear magnetization within hydrated systems in the presence of a selective RF-saturation field and exchange and/or dipolar coupling has followed two general approaches, the use of modified Bloch equations (*16, 22, 25, 39, 43, 44*) and the more general Redfield–Provotorov formalism (*41*). The Bloch equation description lends itself to simplicity with respect to interpretation, comparison between different models accounting for coupled populations and coupling mechanisms, and solving the system of coupled differential equations. The modified Bloch equations are limited in rigor as this formalism is appropriate for mobile populations described by a single T_2 leading to Lorentzian lineshapes for all coupled components (*39, 41*). This is clearly not the case for the semi-solid or solid macromolecular component and leads to limitations in accounting for saturation phenomenon in the macromolecular component. The general "fix" to the Bloch formalism is to introduce a generalized lineshape function appropriate for solid or semi-solid systems into the steady-state solution for the z-component of the macromolecular magnetization (*45, 46*).

The Redfield–Provotorov formalism is a more rigorous approach to solving the response of the solid-like macromolecular spin population to the presence of selective RF-saturation and naturally leads to an arbitrary lineshape function for the solid spins (*41, 47*). Under limiting conditions appropriate to the hydrated macromolecular systems under consideration, the steady-state solution for the bulk-water magnetization approaches that given by the Bloch formalism with the inclusion of an arbitrary lineshape function for the macromolecular population (*41, 47*).

Given the relative simplicity of the Bloch equation formalism, this approach is adopted here to describe a three-pool model for magnetization transfer. The coupled populations presented in Fig. 1 are as follows: (Pool C) hydrogens in the macromolecule. Dipolar coupling in this semi-solid population allows for rapid equilibration of magnetization such that these hydrogens will be considered a single population; (Pool B) solvent hydrogens dipolar-coupled to the macromolecular hydrogen population. These include whole-solvent hydrogens which are anchored in the dipolar coupling site and may also include exchangeable macromolecular hydrogens in the coupling site when the solvent also includes exchangeable hydrogens; (Pool A) all other solvent hydrogens, including solvent hydrogens which exchange in and out of the hydration layer at sites where dipolar coupling to macromolecular hydrogens does not occur. These solvent hydrogens are also considered a single population as a result of efficient exchange and mixing from diffusion. The modified Bloch equations including exchange effects on the transverse components of the bulk- and dipolar-coupled-solvent populations are given by (*48*),

$$
\begin{aligned}
\frac{dM_z^{\mathrm{A}}(t)}{dt} &= \frac{M_0^{\mathrm{A}} - M_z^{\mathrm{A}}(t)}{T_{1\mathrm{A}}} - \kappa_{\mathrm{ex}}^{\mathrm{AB}} M_z^{\mathrm{A}}(t) \\
&\quad + \kappa_{\mathrm{ex}}^{\mathrm{BA}} M_z^{\mathrm{B}}(t) + \omega_1 M_y^{\mathrm{A}}(t) \\
\frac{dM_z^{\mathrm{B}}(t)}{dt} &= \frac{M_0^{\mathrm{B}} - M_z^{\mathrm{B}}(t)}{T_{1\mathrm{B}}} - \kappa_{\mathrm{ex}}^{\mathrm{BA}} M_z^{\mathrm{B}}(t) + \kappa_{\mathrm{ex}}^{\mathrm{AB}} M_z^{\mathrm{A}}(t) \\
&\quad - \kappa_{\mathrm{dip}}^{\mathrm{BC}} M_z^{\mathrm{B}}(t) + \kappa_{\mathrm{dip}}^{\mathrm{CB}} M_z^{\mathrm{C}}(t) + \omega_1 M_y^{\mathrm{B}}(t) \\
\frac{dM_z^{\mathrm{C}}(t)}{dt} &= \frac{M_0^{\mathrm{C}} - M_z^{\mathrm{C}}(t)}{T_{1\mathrm{C}}} - \kappa_{\mathrm{dip}}^{\mathrm{CB}} M_z^{\mathrm{C}}(t) + \kappa_{\mathrm{dip}}^{\mathrm{BC}} M_z^{\mathrm{B}}(t) + \omega_1 M_y^{\mathrm{C}}(t) \\
\frac{dM_x^{\mathrm{A}}(t)}{dt} &= -\frac{M_x^{\mathrm{A}}(t)}{T_{2A}} - \kappa_{\mathrm{ex}}^{\mathrm{AB}} M_x^{\mathrm{A}}(t) + \kappa_{\mathrm{ex}}^{\mathrm{BA}} M_x^{\mathrm{B}}(t) - 2\pi\,\Delta_{\mathrm{A}} M_y^{\mathrm{A}}(t) \\
\frac{dM_x^{\mathrm{B}}(t)}{dt} &= -\frac{M_x^{\mathrm{B}}(t)}{T_{2B}} - \kappa_{\mathrm{ex}}^{\mathrm{BA}} M_x^{\mathrm{B}}(t) + \kappa_{\mathrm{ex}}^{\mathrm{AB}} M_x^{\mathrm{A}}(t) - 2\pi\,\Delta_{\mathrm{B}} M_y^{\mathrm{B}}(t) \\
\frac{dM_x^{\mathrm{C}}(t)}{dt} &= -\frac{M_x^{\mathrm{C}}(t)}{T_{2C}} - 2\pi\,\Delta_{\mathrm{C}} M_y^{\mathrm{C}}(t) \\
\frac{dM_y^{\mathrm{A}}(t)}{dt} &= -\frac{M_y^{\mathrm{A}}(t)}{T_{2A}} - \kappa_{\mathrm{ex}}^{\mathrm{AB}} M_y^{\mathrm{A}}(t) + \kappa_{\mathrm{ex}}^{\mathrm{BA}} M_y^{\mathrm{B}}(t) \\
&\quad + 2\pi\,\Delta_{\mathrm{A}} M_x^{\mathrm{A}}(t) - \omega_1 M_z^{\mathrm{A}}(t) \\
\frac{dM_y^{\mathrm{B}}(t)}{dt} &= -\frac{M_y^{\mathrm{B}}(t)}{T_{2B}} - \kappa_{\mathrm{ex}}^{\mathrm{BA}} M_y^{\mathrm{B}}(t) + \kappa_{\mathrm{ex}}^{\mathrm{AB}} M_y^{\mathrm{A}}(t) \\
&\quad + 2\pi\,\Delta_{\mathrm{B}} M_x^{\mathrm{B}}(t) - \omega_1 M_z^{\mathrm{B}}(t) \\
\frac{dM_y^{\mathrm{C}}(t)}{dt} &= -\frac{M_y^{\mathrm{C}}(t)}{T_{2C}} + 2\pi\,\Delta_{\mathrm{C}} M_x^{\mathrm{C}}(t) - \omega_1 M_z^{\mathrm{C}}(t),
\end{aligned}
\qquad [1]
$$

where $M^i_{x,y,z}$ are the x-, y-, and z-components of the magnetization of the bulk-solvent hydrogens (A), solvent hydrogens bound in the dipolar coupling site (B), and macromolecular hydrogens (C). $\kappa_{ex}^{AB,BA}$ is the hydrogen exchange rate between the bulk-solvent and dipolar-coupled-solvent hydrogens. $\kappa_{dip}^{BC,CB}$ is the through-space dipolar exchange rate between the solvent and macromolecular hydrogens in the coupling site. T_{1A}, T_{2A} and T_{1B}, T_{2B} and T_{1C}, T_{2C} are the spin–lattice and spin–spin relaxation times for the bulk-solvent, dipolar-coupled solvent, and macromolecular hydrogens, respectively. Δ_i is the frequency offset in hertz and ω_1 is the magnitude in rad/s of the saturation field. The effects of dipolar coupling on the transverse components of the dipolar-coupled solvent and macromolecular magnetizations have not been included. As has been previously shown, the inclusion of these factors leads to small corrections to the steady-state bulk-water signal intensity (*43*). Inclusion of these factors also precludes the introduction of the arbitrary lineshape function for the macromolecular population. The steady-state solutions to Eq. [1] are presented in Appendix A.

A further simplification which leads to steady-state solutions which are algebraically simpler to solve and easier to interpret is to eliminate the exchange terms for all of the transverse components,

$$\begin{aligned}
\frac{dM_z^A(t)}{dt} &= \frac{M_0^A - M_z^A(t)}{T_{1A}} - \kappa_{ex}^{AB} M_z^A(t) \\
&\quad + \kappa_{ex}^{BA} M_z^B(t) + \omega_1 M_y^A(t) \\
\frac{dM_z^B(t)}{dt} &= \frac{M_0^B - M_z^B(t)}{T_{1B}} - \kappa_{ex}^{BA} M_z^B(t) + \kappa_{ex}^{AB} M_z^A(t) \\
&\quad - \kappa_{dip}^{BC} M_z^B(t) + \kappa_{dip}^{CB} M_z^C(t) + \omega_1 M_y^B(t) \\
\frac{dM_z^C(t)}{dt} &= \frac{M_0^C - M_z^C(t)}{T_{1C}} - \kappa_{dip}^{CB} M_z^C(t) \\
&\quad + \kappa_{dip}^{BC} M_z^B(t) + \omega_1 M_y^C(t) \\
\frac{dM_x^A(t)}{dt} &= -\frac{M_x^A(t)}{T_{2A}} - 2\pi\Delta_A M_y^A(t) \\
\frac{dM_x^B(t)}{dt} &= -\frac{M_x^B(t)}{T_{2B}} - 2\pi\Delta_B M_y^B(t) \\
\frac{dM_x^C(t)}{dt} &= -\frac{M_x^C(t)}{T_{2C}} - 2\pi\Delta_C M_y^C(t) \\
\frac{dM_y^A(t)}{dt} &= -\frac{M_y^A(t)}{T_{2A}} + 2\pi\Delta_A M_x^A(t) - \omega_1 M_z^A(t) \\
\frac{dM_y^B(t)}{dt} &= -\frac{M_y^B(t)}{T_{2B}} + 2\pi\Delta_B M_x^B(t) - \omega_1 M_z^B(t) \\
\frac{dM_y^C(t)}{dt} &= -\frac{M_y^C(t)}{T_{2C}} + 2\pi\Delta_C M_x^C(t) - \omega_1 M_z^C(t).
\end{aligned} \quad [2]$$

The steady-state solutions for the z-components (longitudinal components) following elimination of the equations for the x- and y-components gives

$$\begin{aligned}
-R_{1A}M_0^A &= -\left(R_{1A} + \kappa_{ex}^{AB} + \frac{\omega_1^2 T_{2A}}{1+(2\pi\Delta_A T_{2A})^2}\right) M_z^A(\infty) \\
&\quad + \kappa_{ex}^{BA} M_z^B(\infty) \\
-R_{1B}M_0^B &= -\left(R_{1B} + \kappa_{ex}^{BA} + \kappa_{dip}^{BC} + \frac{\omega_1^2 T_{2B}}{1+(2\pi\Delta_B T_{2B})^2}\right) M_z^B(\infty) \\
&\quad + \kappa_{ex}^{AB} M_z^A(\infty) + \kappa_{dip}^{CB} M_z^C(\infty) \\
-R_{1C}M_0^C &= -\left(R_{1C} + \kappa_{dip}^{CB} + \frac{\omega_1^2 T_{2C}}{1+(2\pi\Delta_C T_{2C})^2}\right) M_z^C(\infty) \\
&\quad + \kappa_{dip}^{BC} M_z^B(\infty),
\end{aligned} \quad [3]$$

where $R_{1X} = 1/T_{1X}$. It is shown below by comparing the solutions to Eqs. [2] and [1] which are presented in Eqs. [3] and [A1] that it makes little difference to include the exchange terms under the rapid exchange conditions appropriate for the systems under consideration.

The normalized Lorentzian lineshape is given by

$$g^L(2\pi\Delta_i) = \frac{T_{2i}}{\pi}\frac{1}{1+(2\pi\Delta_i T_{2i})^2}. \quad [4]$$

Common practice is to replace the Lorentzian lineshape function which results from the Bloch formalism with a generalized lineshape function for the macromolecular component (*39, 44*). In general, the lineshape of the macromolecular component is well approximated by a Gaussian,

$$g^G(2\pi\Delta_C) = \frac{1}{\sigma_C\sqrt{2\pi}}\exp\left(\frac{-(2\pi\Delta_C)^2}{2\sigma_C^2}\right), \quad [5]$$

where σ_C is the linewidth of the macromolecular hydrogen spectrum. T_{2C} is defined as $1/(\pi\sigma_C)$. Rewriting Eq. [3] by considering the relative longitudinal magnetizations, $M_z^i(\infty)/M_0^i$, and using the following equilibrium conditions and definitions (*25*),

$$\begin{aligned}
M_0^A\kappa_{ex}^{AB} &= M_0^B\kappa_{ex}^{BA}, \quad \frac{M_0^B}{M_0^A} = f_{BA} \\
M_0^B\kappa_{dip}^{BC} &= M_0^C\kappa_{dip}^{CB}, \quad \frac{M_0^B}{M_0^C} = f_{BC},
\end{aligned} \quad [6]$$

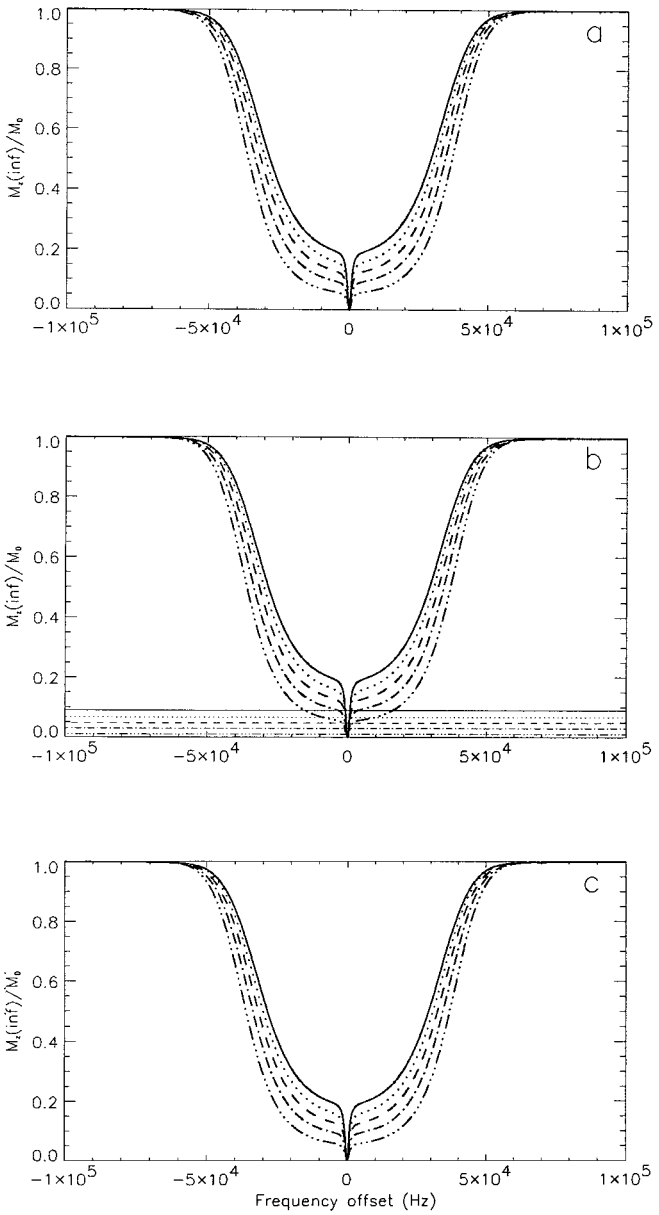

FIG. 2. Magnetization transfer spectra representing the bulk-water steady-state longitudinal magnetization, $M_z^{\mathrm{A}}(\infty)/M_0^{\mathrm{A}}$, as a function of offset frequency for the RF saturation field, Δ. Intensities are normalized to the signal amplitude in the absence of RF saturation. The narrow component near $\Delta = 0$ Hz reflects the direct saturation of the water resonance. The broad component reflects the indirect water–macromolecular magnetization transfer effect. (a)Theoretical MT spectra calculated using the two-pool model presented in Eq. [11]. $\omega_1 =$ 3140 rad/s. Relaxation and population parameters are calculated or entered as ranges reflecting general trends as a function of temperature (—) 273 K; (· · ·) 298 K; (– – –) 323 K; (–·–) 348 K; (–· · ·–) 373 K. f_{BA}, f_{BC}, f_{CA}, and n_{B} are given in Table 1a. The remaining relaxation parameters are given in Table 3a. (b) Theoretical MT spectra calculated using the steady-state results of the three-pool model presented in Eqs. [7, 8]. Parameters are the same as in (a). The corresponding horizontal lines are the maximum magnetization transfer effect under conditions of complete saturation of the macromolecular magnetization, Eq. [16]. (c) Theoretical MT spectra calculated using the three-pool model including exchange effects on the *x* and *y* components for the bulk and coupling site solvent hydrogens, Eq. [A1]. Parameters are the same as in (a).

gives

$$
\begin{aligned}
-R_{1\mathrm{A}} &= -\left(R_{1\mathrm{A}} + \kappa_{\mathrm{ex}}^{\mathrm{AB}} + R_{\mathrm{RFA}}\right)\frac{M_z^{\mathrm{A}}(\infty)}{M_0^{\mathrm{A}}} + \kappa_{\mathrm{ex}}^{\mathrm{AB}}\frac{M_z^{\mathrm{B}}(\infty)}{M_0^{\mathrm{B}}} \\
-R_{1\mathrm{B}} &= -\left(R_{1\mathrm{B}} + \frac{\kappa_{\mathrm{ex}}^{\mathrm{AB}}}{f_{\mathrm{BA}}} + \frac{\kappa_{\mathrm{dip}}^{\mathrm{CB}}}{f_{\mathrm{BC}}} + R_{\mathrm{RFB}}\right)\frac{M_z^{\mathrm{B}}(\infty)}{M_0^{\mathrm{B}}} \\
&\quad + \frac{\kappa_{\mathrm{ex}}^{\mathrm{AB}}}{f_{\mathrm{BA}}}\frac{M_z^{\mathrm{A}}(\infty)}{M_0^{\mathrm{A}}} + \frac{\kappa_{\mathrm{dip}}^{\mathrm{CB}}}{f_{\mathrm{BC}}}\frac{M_z^{\mathrm{C}}(\infty)}{M_0^{\mathrm{C}}} \qquad [7] \\
-R_{1\mathrm{C}} &= -\left(R_{1\mathrm{C}} + \kappa_{\mathrm{dip}}^{\mathrm{CB}} + R_{\mathrm{RFC}}\right)\frac{M_z^{\mathrm{C}}(\infty)}{M_0^{\mathrm{C}}} + \kappa_{\mathrm{dip}}^{\mathrm{CB}}\frac{M_z^{\mathrm{B}}(\infty)}{M_0^{\mathrm{B}}} \\
R_{\mathrm{RF}i} &= \omega_1^2\pi g^{\mathrm{L}}(2\pi\Delta_i), \quad i = \mathrm{A}, \mathrm{B} \\
R_{\mathrm{RFC}} &= \omega_1^2\pi g^{\mathrm{G}}(2\pi\Delta_{\mathrm{C}}).
\end{aligned}
$$

It is important to recognize that the conditions given in Eq. [6] for dipolar coupling are a consequence of using $\kappa_{\mathrm{dip}}^{\mathrm{BC,CB}}$ to describe the pseudo-first-order rate constants for *inter*molecular dipolar coupling (*16*, *25*, *49*). It is straightforward, but cumbersome to solve this set of linear equations for the bulk-solvent equilibrium magnetization, $M_z^{\mathrm{A}}(\infty)/M_0^{\mathrm{A}}$. As the approach here is to model trends in empirical data and set constraints on the parameters, rather than to fit the data and extract parameters, the analytical solution for $M_z^{\mathrm{A}}(\infty)/M_0^{\mathrm{A}}$ is not needed. The above set of linear equations is solved here numerically for $M_z^{\mathrm{A}}(\infty)/M_0^{\mathrm{A}}$, $M_z^{\mathrm{B}}(\infty)/M_0^{\mathrm{B}}$, and $M_z^{\mathrm{C}}(\infty)/M_0^{\mathrm{C}}$ as a function of saturation frequency offset, Δ, using Cramer's rule as provided in the programming language IDL (Research Systems, Inc., Boulder, CO). The $M_z^{\mathrm{A}}(\infty)/M_0^{\mathrm{A}}$ output is a magnetization transfer spectrum (also referred to as a *Z*-spectrum (*33*)) of the bulk-solvent equilibrium signal intensity as a function of the frequency offset of the saturation field, Δ; see Fig. 2. The relatively narrow dip near $\Delta = 0$ Hz reflects the direct saturation of the solvent resonance. The broad shape of the MT spectrum reflects the indirect solvent–macromolecular magnetization transfer and is also a measure of the lineshape of the macromolecular hydrogen population to which the solvent hydrogens are coupled. The depth of the MT spectrum is a function of the magnitude of water–macromolecular hydrogen coupling, relative hydrogen populations, and relaxation parameters for each population.

One of the goals of the present work is to assess the appropriateness of a two-pool model to describe magnetization transfer. To facilitate the comparison between the results starting from an explicit three-pool model and results obtained using a two-pool model characterizing coupling between the bulk-solvent and macromolecular populations, $M_z^{\mathrm{B}}(\infty)/M_0^{\mathrm{B}}$ in Eqs. [7] can be eliminated by solving the second of Eqs. [7] for $M_z^{\mathrm{B}}(\infty)/M_0^{\mathrm{B}}$ in terms of $M_z^{\mathrm{A}}(\infty)/M_0^{\mathrm{A}}$ and $M_z^{\mathrm{C}}(\infty)/M_0^{\mathrm{C}}$. The solution for $M_z^{\mathrm{B}}(\infty)/M_0^{\mathrm{B}}$ can then be substituted into the first and third of Eqs. [7], leaving two equations characterizing the equilibrium magnetization in the bulk-solvent and macromolecular

populations,

$$
\begin{aligned}
-R_{1A} - \left(\frac{\kappa_{ex}^{AB}}{R_B}\right) R_{1B} &= -\left(R_A - \frac{\left(\kappa_{ex}^{AB}\right)^2}{f_{BA} R_B}\right) \frac{M_z^A(\infty)}{M_0^A} \\
&\quad + \left(\frac{\kappa_{ex}^{AB}\kappa_{dip}^{CB}}{f_{BC} R_B}\right) \frac{M_z^C(\infty)}{M_0^C} \\
-R_{1C} - \left(\frac{\kappa_{dip}^{CB}}{R_B}\right) R_{1B} &= -\left(R_C - \frac{\left(\kappa_{dip}^{CB}\right)^2}{f_{BC} R_B}\right) \frac{M_z^C(\infty)}{M_0^C} \\
&\quad + \left(\frac{\kappa_{ex}^{AB}\kappa_{dip}^{CB}}{f_{BA} R_B}\right) \frac{M_z^A(\infty)}{M_0^A}, \qquad [8] \\
R_A &= \left(R_{1A} + \kappa_{ex}^{AB} + R_{RFA}\right) \\
R_B &= \left(R_{1B} + \frac{\kappa_{ex}^{AB}}{f_{BA}} + \frac{\kappa_{dip}^{CB}}{f_{BC}} + R_{RFB}\right) \\
R_C &= \left(R_{1C} + \kappa_{dip}^{CB} + R_{RFC}\right).
\end{aligned}
$$

This form of Eqs. [7] will be referred to as the reduced three-pool model. It explicitly couples the macromolecular and bulk populations and includes the effects and properties of the dipolar-coupled solvent hydrogens. The coupling constant between the bulk-solvent and macromolecular populations, κ^{AC}, is given by

$$
\kappa^{AC} = \left(\frac{\kappa_{ex}^{AB}\kappa_{dip}^{CB}}{f_{BC} R_B}\right). \qquad [9]
$$

The two-pool model for coupling between bulk-solvent and macromolecular populations is described by the following set of coupled differential equations,

$$
\begin{aligned}
\frac{dM_z^A(t)}{dt} &= \frac{M_0^A - M_z^A(t)}{T_{1A}} - \kappa_{eff}^{AC} M_z^A(t) + \kappa_{eff}^{CA} M_z^C(t) + \omega_1 M_y^A(t) \\
\frac{dM_z^C(t)}{dt} &= \frac{M_0^C - M_z^C(t)}{T_{1C}} - \kappa_{eff}^{CA} M_z^C(t) + \kappa_{eff}^{AC} M_z^A(t) + \omega_1 M_y^C(t) \\
\frac{dM_x^A(t)}{dt} &= -\frac{M_x^A(t)}{T_{2A}} - 2\pi\Delta_A M_y^A(t) \\
\frac{dM_x^C(t)}{dt} &= -\frac{M_x^C(t)}{T_{2C}} - 2\pi\Delta_C M_y^C(t) \qquad [10] \\
\frac{dM_y^A(t)}{dt} &= -\frac{M_y^A(t)}{T_{2A}} + 2\pi\Delta_A M_x^A(t) - \omega_1 M_z^A(t) \\
\frac{dM_y^C(t)}{dt} &= -\frac{M_y^C(t)}{T_{2C}} + 2\pi\Delta_C M_x^C(t) - \omega_1 M_z^C(t).
\end{aligned}
$$

The solution of Eqs. [10] leads to the following set of linear equations for the steady-state magnetizations, $M_z^A(\infty)/M_0^A$ and $M_z^C(\infty)/M_0^C$ (*39*),

$$
\begin{aligned}
-R_{1A} &= -\left(R_{1A} + \kappa_{eff}^{AC} + R_{RFA}\right) \frac{M_z^A(\infty)}{M_0^A} + \kappa_{eff}^{AC} \frac{M_z^C(\infty)}{M_0^C} \qquad [11] \\
-R_{1C} &= -\left(R_{1C} + \frac{\kappa_{eff}^{AC}}{f_{CA}} + R_{RFC}\right) \frac{M_z^C(\infty)}{M_0^C} + \frac{\kappa_{eff}^{AC}}{f_{CA}} \frac{M_z^A(\infty)}{M_0^A},
\end{aligned}
$$

where the following equilibrium condition and definition were used,

$$
M_0^A \kappa_{eff}^{AC} = M_0^C \kappa_{eff}^{CA}, \quad \frac{M_0^C}{M_0^A} = f_{CA}. \qquad [12]
$$

The two-pool model is a good approximation to the three-pool model under conditions where the **B** population is small (f_{BA} and $f_{BC} \ll 1$) and when κ_{eff}^{AC} in the two-pool model is defined as in Eq. [9]. Under these conditions, the following approximations for terms in the reduced three-pool model Eq. [8] are valid,

$$
\begin{aligned}
R_B = \left(R_{1B} + \frac{\kappa_{ex}^{AB}}{f_{BA}} + \frac{\kappa_{dip}^{CB}}{f_{BC}} + R_{RFB}\right) &\approx \left(\frac{\kappa_{ex}^{AB}}{f_{BA}} + \frac{\kappa_{dip}^{CB}}{f_{BC}}\right), \\
\frac{\kappa_{ex}^{AB}}{R_B} &\approx \frac{\kappa_{ex}^{AB}}{\left(\frac{\kappa_{ex}^{AB}}{f_{BA}} + \frac{\kappa_{dip}^{CB}}{f_{BC}}\right)} \ll 1, \qquad [13] \\
\frac{\kappa_{dip}^{CB}}{R_B} &\approx \frac{\kappa_{dip}^{CB}}{\left(\frac{\kappa_{ex}^{AB}}{f_{BA}} + \frac{\kappa_{dip}^{CB}}{f_{BC}}\right)} \ll 1,
\end{aligned}
$$

and Eq. [8] is well approximated by the results of the two-pool model in Eq. [11].

As expected for a series coupled system, the coupling constant from the reduced three-pool model, κ^{AC}, will be limited by the smaller of the rate constants, κ_{ex}^{AB} and κ_{dip}^{CB},

$$
\begin{aligned}
\kappa^{AC} = \left(\frac{\kappa_{ex}^{AB}\kappa_{dip}^{CB}}{f_{BC} R_B}\right) &\approx \left(\frac{\kappa_{ex}^{AB}\kappa_{dip}^{CB}}{f_{BC}\left(\frac{\kappa_{ex}^{AB}}{f_{BA}} + \frac{\kappa_{dip}^{CB}}{f_{BC}}\right)}\right) \\
\kappa^{AC} &\approx f_{CA}\kappa_{dip}^{CB} \quad \text{when } \kappa_{ex}^{AB} \gg \kappa_{dip}^{CB}, \qquad [14] \\
\kappa^{AC} &\approx \kappa_{ex}^{AB} \quad \text{when } \kappa_{dip}^{CB} \gg \kappa_{ex}^{AB}.
\end{aligned}
$$

The coupling constant is a function of the relative sizes of the macromolecular and bulk-solvent populations when the exchange rate is large, and independent of the relative amounts of the coupled populations under conditions when the dipolar coupling rate is large relative to the exchange rate.

When both κ_{ex}^{AB} and κ_{dip}^{CB} are large relative to R_{1A}, R_{1C}, R_{RFA}, and R_{RFC} and the size of the dipolar-coupled solvent population is small, f_{BA} and $f_{BC} \ll 1$, the steady-state bulk-solvent

magnetization in the presence of RF-saturation is independent of the coupling rates and is limited by f_{CA}, R_{1A}, R_{1C}, R_{RFA}, and R_{RFC}. Starting from Eq. [11] which approximates the solution to the three-pool model under the conditions of a small intermediate population and solving for $M_z^A(\infty)/M_0^A$,

$$\frac{M_z^A(\infty)}{M_0^A} = \frac{-R_{1A} - \frac{\kappa^{AC} R_{1C}}{R_C}}{-R_A R_C + \frac{(\kappa^{AC})^2}{f_{CA}}} \approx \frac{1}{1 + \frac{f_{CA} R_{RFC} + R_{RFA}}{R_{1A} + f_{CA} R_{1C}}}$$
$$\text{when} \quad \frac{\kappa^{AC}}{f_{CA}} \gg R_{1C}, R_{RFC}. \qquad [15]$$

A final limit considered here for $M_z^A(\infty)/M_0^A$ is that under conditions of complete saturation of the macromolecular magnetization, $M_z^C(\infty) = 0$, which gives the maximum possible magnetization transfer effect. From Eq. [8], when $M_z^C(\infty) = 0$,

$$\frac{M_z^A(\infty)}{M_0^A} = \frac{R_{1A} + \left(\frac{\kappa_{ex}^{AB}}{R_B}\right) R_{1B}}{\left(R_A - \frac{\left(\kappa_{ex}^{AB}\right)^2}{f_{BA} R_B}\right)} = \frac{R_{1A} R_B + \kappa_{ex}^{AB} R_{1B}}{\left(R_A R_B - \frac{\left(\kappa_{ex}^{AB}\right)^2}{f_{BA}}\right)}. \qquad [16]$$

Equation [17] gives the enhancement factor (*34*),

$$\frac{M_z^A(\infty) - M_0^A}{M_0^A} = \frac{-\kappa_{ex}^{AB} \kappa_{dip}^{CB}}{\left(R_A R_B - \frac{\left(\kappa_{ex}^{AB}\right)^2}{f_{BA}}\right)}. \qquad [17]$$

(*Note.* κ_{dip} in Ref. *34* is equivalent to κ_{dip}^{BC} in the present work.)

Parameter Calculation and Constraints

The equilibrium bulk-solvent signal intensity, $M_z^A(\infty)/M_0^A$, will depend on the T_1's and T_2's of each population, f_{BA} and f_{BC}, κ_{ex}^{AB} and κ_{dip}^{CB}, and ω_1, Δ_A, Δ_B, Δ_C. ω_1 is set experimentally. Under conditions where the spectrometer frequency is set on- resonance for the water signal, Δ_A is the offset frequency of the saturation field. Δ_B and Δ_C will be offset from Δ_A by the chemical shift differences δ_{AB} and δ_{AC}, respectively. The water in the coupling site will most likely be held there through hydrogen bonding which will shift the bound-water resonance downfield. Empirical data show that the center of the broad resonance from the macromolecular population is shifted upfield from the bulk-water resonance. δ_{AB} and δ_{AC} are approximated here as -3.3 and 1.5 ppm (-1000 and 500 Hz at a field strength of 300 MHz). The chemical shifts are relatively unimportant, affecting only the width of the narrow dip near $\Delta \sim 0$ Hz, reflecting the direct saturation of the solvent resonance.

The remaining parameters must be determined by fitting experimental magnetization transfer data. A starting point to modeling magnetization transfer data is to establish reasonable approximations and constraints to the parameters in Eqs. [7, 8], [11], and [A1] consistent with experimental MT results and which leave the dimensions of the undetermined parameter space relatively small. The coupling constants and relaxation parameters are all dependent on dynamics within the hydrated systems and therefore will be sensitive to temperature. Although not necessarily clinically applicable, the effect of temperature on these parameters can be modeled and used to further establish how the parameters may limit the observable magnetization transfer effect in both clinical and nonclinical systems.

Relative hydrogen populations. The dependence of the equilibrium bulk-solvent magnetization on the relative amounts in the bulk-solvent, dipolar-coupled solvent, and macromolecular populations enters through the parameters f_{BA}, f_{BC}, and f_{CA}. Based on the observation of a single broad resonance for the macromolecular hydrogens, the argument is made here that the C-pool behaves as a single population as a result of efficient dipolar mixing. The bulk-solvent hydrogens are considered a single population as a result of efficient mixing from diffusion. To simplify the model, the hydrogens in the dipolar coupling sites will also be considered a single population. This is certainly an approximation, especially in protein systems where it is likely that coupling sites will differ in structure and conformation. It would be straightforward to include characteristically different coupling sites. However, this seems a reasonable simplification since an objective of the present work is to place constraints on the parameters rather than to solve for them explicitly. Estimates of f_{BA}, f_{BC}, and f_{CA} are then straightforward, given that the sample composition and number of coupling sites on the macromolecular surface are known. The temperature dependence of f_{BA}, f_{BC}, and f_{CA} enters through the equilibrium conditions (*28, 50*),

$$nL_{free} + S_{free} \rightleftarrows L_n S,$$
$$K_b^c = \frac{[L_n S]}{[L_{free}]^n [S_{free}]} = \frac{[L_{bound}]}{[L_{free}]^n [S_{free}]}, \qquad [18]$$
$$\ln \frac{K_{b,1}^c}{K_{b,2}^c} = -\frac{\Delta H_b}{R}\left(\frac{1}{T_2} - \frac{1}{T_1}\right),$$

where L represents the ligand or solvent, S represents the solute or macromolecule, K_b^c is the concentration binding constant, and ΔH_b is the enthalpy of binding. n is the number of dipolar coupling sites on each macromolecule. The assumption is made here that these sites are equivalent. This assumption is valid in lipid bilayer systems, but is a simplification for protein systems where these sites may certainly differ in both structure and dynamics. f_{BA}, f_{BC}, and f_{CA} can be determined as a function of temperature by first solving Eq. [18] for $[L_{bound}]$ as a function of K_b^c. Rewriting the equilibrium expression in terms of $[L_{bound}]$

and K_b^c,

$$K_b^c = \frac{[L_{bound}]}{([L_{total}] - [L_{bound}])^n ([S_{total}] - [S_{bound}])} = \frac{[L_{bound}]}{([L_{total}] - [L_{bound}])^n \left([S_{total}] - \frac{[L_{bound}]}{n}\right)} \quad [19]$$

results in a general polynomial expression in $[L_{bound}]$ as a function of K_b^c, $[L_{total}]$, $[S_{total}]$, and n,

$$K_b^c[L_{tot}]^n[S_{tot}] - \left(K_b^c[L_{tot}]^{n-1}\left(B_{n,1}\frac{[L_{tot}]}{n} + B_{n,2}[S_{tot}]\right) + 1\right)[L_{bound}] + \sum_{i=2}^{n}(-1)^i K_b^c[L_{tot}]^{n-i}\left(B_{n,i}\frac{[L_{tot}]}{n} + B_{n,i+1}[S_{tot}]\right) \times [L_{bound}]^i + (-1)^{n+1}K_b^c\frac{1}{n}[L_{bound}]^{n+1} = 0. \quad [20]$$

$B_{n,i}$ are the coefficients of the binomial expansion. The roots of Eq. [20] were found using Laguerre's method as provided in the data language IDL. The relevant root was chosen as that between 0 and the maximum ligand bound concentration. Given $[L_{bound}]$, the parameters f_{BA}, f_{BC}, and f_{CA} can be calculated using the relationships

$$f_{BA} = \frac{[L_{bound}]}{[L_{free}]}, \quad f_{BC} = \frac{[L_{bound}] \times N_H^L}{[S_{tot}] \times N_H^S}, \quad f_{CA} = \frac{f_{BA}}{f_{BC}}, \quad [21]$$

$$f_{CA}^{min} = \frac{[S_{tot}] \times N_H^S}{[L_{tot}] \times N_H^L}, \quad f_{CA}^{max} = \frac{[S_{tot}] \times N_H^S}{([L_{tot}] - n[S_{tot}]) \times N_H^L},$$

where N_H^L and N_H^S are the number of hydrogens per solvent and macromolecule, respectively, and f_{CA}^{max} and f_{CA}^{min} are the maximum and minimum values of f_{CA}, respectively. Sample results are given in Table 1 as a function of $K_{b,1}^c$, ΔH_b, n, $[L_{tot}]$, and $[S_{tot}]$. It is important to note that f_{CA} changes very little with temperature; see Table 1b. If the solvent is diluted with a deuterated solvent, the bound fraction of solvent will stay the same, which means f_{BA} will not change. The fraction f_{BC} will decrease by the dilution factor, and therefore, f_{CA} will increase by the same factor; see Table 1c. It should be noted that the effects of isotopic dilution of the solvent on the number of macromolecular hydrogens are not accounted for here. In lipids, the change in the number of macromolecular hydrogens as a result of isotopic substitution by labile hydrogen exchange will be small. In proteins, this may account for up to 5% of the hydrogens.

Spin–lattice and spin–spin relaxation. The relaxation parameters, R_{1A}, R_{1B}, R_{1C}, T_{2A}, T_{2B}, and T_{2C} (or $1/\sigma_C$), will vary

TABLE 1
n_B, f_{BA}, f_{BC}, and f_{CA} as a Function of Temperature

Temperature	K_b^c	$[L_{bound}]$	n_B	f_{BA}	f_{BC}	f_{CA}
		$n = 5$ $[L_{tot}] = 40$ M				
		$\Delta H_b = -40$ kJ $[S_{tot}] = 1 \times 10^{-3}$ M				
		dilution factor = 1.0				
273	1.00	0.00500	10	0.000125	0.00167	0.0750
298	0.228	0.00500	10	0.000125	0.00167	0.0750
323	0.0653	0.00500	10	0.000125	0.00167	0.0750
348	0.0334	0.00500	10	0.000125	0.00167	0.0750
373	0.00887	0.00500	10	0.000125	0.00167	0.0750
		$n = 5$ $[L_{tot}] = 40$ M				
		$\Delta H_b = -40$ kJ $[S_{tot}] = 1 \times 10^{-3}$ M				
		dilution factor = 1.0				
273	1.00×10^{-6}	0.00477	9.53	0.000119	0.00159	0.0750
298	0.228×10^{-6}	0.00412	8.24	0.000103	0.00137	0.0750
323	0.0653×10^{-6}	0.00286	5.72	7.15×10^{-5}	0.000954	0.0750
348	0.0334×10^{-6}	0.00157	3.15	3.93×10^{-5}	0.000524	0.0750
373	0.00887×10^{-6}	0.000769	1.54	1.92×10^{-5}	0.000256	0.0750
		$n = 5$ $[L_{tot}] = 40$ M				
		$\Delta H_b = -40$ kJ $[S_{tot}] = 1 \times 10^{-3}$ M				
		dilution factor = 0.1				
273	1.00×10^{-6}	0.00477	0.95	0.000125	0.000167	0.750
298	0.228×10^{-6}	0.00412	0.82	0.000125	0.000167	0.750
323	0.0653×10^{-6}	0.00286	0.57	0.000125	0.000167	0.750
348	0.0334×10^{-6}	0.00157	0.32	0.000125	0.000167	0.750
373	0.00887×10^{-6}	0.000769	0.15	0.000125	0.000167	0.750

Note. The data presented are for a system 1×10^{-3} M in protein which approximates a 10% by mass sample of albumin in water. $N_H^L = 2$, $N_H^S = 6000$.

with the correlation times describing the motions of the hydrogens in the A-pool (bulk solvent), B-pool (dipolar coupled solvent hydrogens), and C-pool (macromolecular hydrogens), τ_{bulk}, τ_{site}, τ_{mac}, respectively. Relevant motions include rotation and translation of solvent molecules in the bulk phase, restricted rotation and translation of solvent hydrogens in the coupling site on the macromolecular surface, and restricted motions in the macromolecular matrix (*51–53*).

The temperature dependence of diffusion for water in hydrated macromolecular systems has been shown to follow Arrhenius-like behavior with activation energies on the order of 20 kJ mol^{-1} (*54, 55*). The temperature dependence of the rotational and translational diffusion correlation times can be estimated as

$$\ln\left(\frac{\tau_{\text{bulk}}(373\text{ K})}{\tau_{\text{bulk}}(273\text{ K})}\right) = \frac{-E_a}{R}\left(\frac{1}{273\text{ K}} - \frac{1}{373\text{ K}}\right),$$

$$\frac{\tau_{\text{bulk}}(373\text{ K})}{\tau_{\text{bulk}}(273\text{ K})} \sim 10$$

where E_a is the activation energy and R is the gas constant. Rotation and translation in the bulk phase will be sufficiently fast such that $\tau_{\text{bulk}} \ll 1/\omega_0$ at spectrometer frequencies ~100 MHz. Under these conditions, $T_{1A} \propto 1/\tau_{\text{bulk}}$. The upper limit to T_{1A} will be the spin–lattice relaxation time of the pure solvent. The lower limit to T_{1A} will be the *observed* T_1 of the solvent in the solvated macromolecular system (*41*). $T_{1\text{obs}}$ includes the effects of physical exchange and dipolar coupling which will both make $T_{1\text{obs}}$ shorter than T_{1A}. T_{2A} will increase with $1/\tau_{\text{bulk}}$. Estimates of T_{2A} can be taken as $T_{2\text{obs}}$ for the bulk solvent in the solvated macromolecular system (*39*).

Considering hydrated cross-linked proteins and polymers, the overall mobility of the supramolecular matrix will be relatively rigid, $\tau_{\text{mac}} \gg 1/\omega_0$, ($\tau > 5 \times 10^{-10}$ s at 300 MHz). However, mobile functional groups within the supramolecular matrix, such as rotating methyl groups within proteins and reorienting lipid molecules within bilayers, may reorient on timescales faster than the overall reorientation of the supramolecular matrix (*52, 56, 57*). These functional groups then provide relaxation sinks for the macromolecular hydrogens. The motions of these functional groups will be more restricted in cross-linked proteins and in lipid bilayers than in the solutions of the biopolymers and may range from picoseconds to microseconds. Initial estimates for T_{1C} will be taken from the literature based on the extraction of parameters from empirical MT data (*39, 41, 44*). The inverse of the MT linewidth provides an estimate of the lower limit for T_{2C} which is taken to be on the order of tens of microseconds. The approximation is made here that T_{2C} varies little with temperature. This assumption is supported by MT studies on cross-linked albumin where the MT spectrum linewidth varies insignificantly as a function of temperature (*28, 42*).

The motions of the solvent hydrogens in the dipolar coupling site will likely be more restricted than in the bulk, so the correlation times τ_{site} would be longer than τ_{bulk}. The temperature dependence of τ_{site} may be stronger or weaker than for τ_{bulk} depending on how the solvent is held in the coupling site. It is difficult to predict whether τ_{site} would be in the long or short correlation time limit, $\tau_{\text{site}} > 1/\omega_0$ or $\tau_{\text{site}} < 1/\omega_0$, respectively, and hence it is difficult to predict the dependence of T_{1B} on τ_{site}. Since $\tau_{\text{bulk}} < \tau_{\text{site}} < \tau_{\text{mac}}$, T_{1B} must be shorter than either T_{1A} or T_{1C} or both. T_{2B} will be longer than T_{2C} and shorter than T_{2A}. As will be shown under Results, the equilibrium bulk-solvent magnetization, M_z^A/M_0^A, has a negligible dependence on T_{1B} and T_{2B} when f_{BA} is small.

Solvent hydrogen exchange rate. Characterization of the rate for physical exchange between the bulk and coupling site populations depends on the mechanism of the exchange process. The exchange rate, κ_{ex}, will be limited by the slower of solvent diffusion and physical exchange at the dipolar coupling site. The approximation is made here that diffusion is rapid enough to keep the solvent population well mixed and will not limit the rate of physical exchange. A single resonance is observed for the solvent hydrogens from both the bulk and the coupling site populations. This suggests that the exchange rate must be fast compared to the chemical shift difference (2000–10,000 s^{-1}) (*10, 18*).

In systems where exchangeable hydrogens are present on both the macromolecular and the solvent molecules, exchange may incorporate the solvent hydrogen into the macromolecular population, and the dipolar coupling occurs between the hydrogen donor and macromolecular hydrogens. The rate of hydrogen exchange will be limited by the strength of the H–X bonds (on the order of hundreds of kilojoules (mol H–X bond)$^{-1}$) and by macromolecular conformation and structure which may restrict exchange. The temperature dependence will be characterized by Arrhenius behavior. Activation energies have been reported ranging from 20 to 400 kJ/mol (*35, 58, 59*). Hydrogen exchange rates in amino acids and peptides have been found to be on the order of 10–10,000 s^{-1} (*35, 60, 61*). In proteins, the amide hydrogen exchange rates are slower by several orders of magnitude (*58, 59, 62*).

Where dipolar transfer is directly between the solvent and macromolecular hydrogens, physical exchange describes the exchange of whole-solvent molecules at the hydrogen-donor functionality in the dipolar-coupling site. The activation energy for the solvent exchange will depend on the interactions holding the solvent molecule at the site which may include structural restrictions and intermolecular hydrogen bonds and dipole–dipole interactions. For hydrogen bonds, E_a may be up to 40 kJ (mol H–bond)$^{-1}$ and will be smaller for fixed dipole–dipole interactions. There is evidence for long-lived water molecules in restricted sites of proteins and lipid bilayers with solvent exchange rates on the order of 10^4–10^6 s^{-1} (*11, 18, 59, 63*).

Dipolar exchange rate. The rate of dipolar magnetization transfer is modeled here based on the Solomon equations for dipolar coupling between two like spins (*16, 17, 21*). The

two-spin dipolar coupling rate is given by

$$-\kappa_{\text{dip}} = W_2 - W_0$$

$$W_2 = \frac{3}{5}\frac{\gamma^4\hbar}{r^6}\left(\frac{\tau_{\text{site}}}{1+\omega_0^2\tau_{\text{site}}^2}\right) \quad W_0 = \frac{1}{10}\frac{\gamma^4\hbar}{r^6}\tau_{\text{site}}, \qquad [22]$$

where W_2 and W_0 are the double- and zero-quantum transition probabilities. τ_{site} will be the shorter of the correlation times describing motions within the restricted site, and τ_{ex} ($=1/\kappa_{\text{ex}}$). It seems likely given the data for solvent and labile hydrogen exchange rates, that τ_{site} will be dominated by motions within the restricted site. For τ_{site} in the long correlation time limit $\tau_{\text{site}} \gg 1/\omega_0$, $W_0 > W_2$, κ_{dip} will be positive, and the enhancement of the bulk-solvent signal intensity upon saturation of the macromolecular magnetization will be negative. To date, there have been no reported cases where a positive enhancement of the bulk-water signal intensity has been observed which limits τ_{site} and therefore κ_{dip}. At 300 MHz, τ_{site} must be longer than 5.93×10^{-10} s to observe negative enhancement ($\kappa_{\text{dip}} > 0\ \text{s}^{-1}$). Negative enhancement in heat-denatured ovalbumin has been observed at 4.2 MHz which limits τ_{site} in that system to longer than 5×10^{-8} s ($\kappa_{\text{dip}} > 12\ \text{s}^{-1}$) (*34*).

The slow limit for τ_{site}, is related to the linewidth of the macromolecular spectrum (*19*). κ_{dip} cannot be greater than the spin–spin relaxation rate within the macromolecular population. For T_{2C} on the order of tens of microseconds, κ_{dip} must be smaller than tens of kilohertz. Based on Eqs. [*22*], τ_{site} must be shorter than 2.5×10^{-4} s.

$\kappa_{\text{dip}}^{\text{BC}}$ and $\kappa_{\text{dip}}^{\text{CB}}$ as used here in Eq. [1] are pseudo-first-order rate constants for intermolecular dipolar magnetization transfer. They are related to κ_{dip} by the relative numbers of interacting hydrogens (*16, 25, 49*),

$$\kappa_{\text{dip}}^{\text{BC}} = n_{\text{C}}\kappa_{\text{dip}}$$

$$\kappa_{\text{dip}}^{\text{CB}} = n_{\text{B}}\kappa_{\text{dip}},$$

where n_{B} is equal to the number of solvent hydrogens per macromolecule which are dipolar coupled in the restricted sites, and n_{C} is the number of hydrogens per macromolecule. n_{B} is given by

$$n_{\text{B}} = \frac{[L_{\text{bound}}] \times N_{\text{H}}^{\text{L}} \times \text{dilution factor}}{[S_{\text{tot}}]},$$

where $[L_{\text{bound}}]$, $[S_{\text{tot}}]$, and N_{H}^{L} are described in Eq. [18]. The dilution factor is associated with isotopic dilution of the solvent and is equal to the ratio of protonated to deuterated solvent. n_{B} may decrease due to isotopic dilution or an increase in temperature; see Table 1. For isotopic dilution, κ_{dip} will remain constant, and $\kappa_{\text{dip}}^{\text{CB}}$ will decrease linearly with the dilution factor. As f_{CA} will increase linearly with the dilution factor, $\kappa^{\text{AC}} = f_{\text{CA}}\kappa_{\text{dip}}^{\text{CB}}$ will remain constant; see Eq. [14]. With an increase in temperature, n_{B} will decrease for small K_{b}^{c} and large ΔH_{b}. f_{CA} stays nearly constant with temperature. $f_{\text{CA}}\kappa_{\text{dip}}^{\text{CB}}$ will then decrease with temperature as both n_{B} and κ_{dip} get smaller with temperature.

RESULTS AND DISCUSSION

Comparison of Two- and Three-Pool Model Results

Magnetization transfer spectra as calculated using the two-pool model, Eq. [11], and three-pool model without, Eqs. [7, 8], and with exchange effects on the *x*- and *y*-components of the bulk and intermediate magnetizations, Eq. [A1], are presented in Fig. 2. There are no detectable differences between the results. Possible differences may arise in the region around $\Delta_{\text{A}} = 0$ where direct saturation of the bulk-solvent magnetization dominates the MT lineshape. In the three-pool model, the effects of exchange between the bulk and coupling site hydrogens may become apparent in a broadening of the central shape of the MT spectrum.

As shown in Eqs. [7–12], the effect of solvent–macromolecular coupling reflected in the broad component of the MT spectrum is apparently well-approximated by the two-pool model with the effective coupling constant, $\kappa_{\text{eff}}^{\text{AC}}$, defined from the results of the reduced three-pool model, Eq. [8]. Other definitions for the effective magnetization transfer coupling constant have been introduced into the two-pool model (*19, 28*). Hinton and Bryant (*28*) define their two-pool magnetization transfer coupling constant, $\kappa_{\text{eff}}^{\text{AC}}$, by

$$\kappa_{\text{eff}}^{\text{AC}} = R_{\text{T}}^{\text{LS}} = \frac{P_i}{T_{IS} + \tau_i}, \qquad [23]$$

where L and S are solvent and macromolecule, respectively, T_{IS}^{-1} is the rate for dipolar exchange in the coupling site with I and S symbolizing the two nonequivalent spins, τ_i is the lifetime of the solvent hydrogen in the dipolar coupling site, and P_i is the probability that the solvent hydrogen is bound in the site. In the notation used in here, $P_i = f_{\text{BA}}$ and $\tau_i = 1/\kappa_{\text{ex}}^{\text{BA}}$. Formally, T_{IS} is the lifetime for two-spin dipolar transfer, or $1/\kappa_{\text{dip}}$ (*51, 64*), which means Eqs. [14] and [23] are not equivalent. However, if T_{IS} is taken as the lifetime for intermolecular dipolar transfer, or $1/\kappa_{\text{dip}}^{\text{BC}}$, the definition in Eq. [23] rewritten in the notation used in the present work gives

$$R_{\text{T}}^{\text{LS}} = R_{\text{T}}^{\text{AB}} = \frac{f_{\text{BA}}}{\frac{1}{\kappa_{\text{dip}}^{\text{BC}}} + \frac{1}{\kappa_{\text{ex}}^{\text{BA}}}} = \frac{f_{\text{BA}}}{\frac{f_{\text{BC}}}{\kappa_{\text{dip}}^{\text{CB}}} + \frac{f_{\text{BA}}}{\kappa_{\text{ex}}^{\text{AB}}}} = \frac{\kappa_{\text{ex}}^{\text{AB}}\kappa_{\text{dip}}^{\text{CB}}}{f_{\text{AC}}\kappa_{\text{ex}}^{\text{AB}} + \kappa_{\text{dip}}^{\text{CB}}}, \qquad [24]$$

which is the same as κ^{AC} from the reduced three-pool model given in Eq. [14] for the condition of a small population of hydrogens in the coupling site.

Hinton and Bryant argue that the dynamics of the solvent hydrogens in the coupling site are the same as those of the macromolecular matrix and use this argument to equate T_{IS} to T_{2C} (*28*). Mathematically, this is consistent since in the long

correlation time limit, both $1/T_{IS}$ and $1/T_{2C}$ will be proportional to τ_{site}. One of the implications of this equivalence is that T_{IS} is equal to the reciprocal of the intrinsic dipolar rate, $1/\kappa_{dip}$, not the intermolecular dipolar rate, $1/\kappa_{dip}^{BC}$. If T_{IS} is equated to $1/\kappa_{dip}$, Eqs. [23] and [24] cannot be made equivalent. Further, from Eq. [22], identifying T_{IS} with $1/\kappa_{dip}$ implies that τ_{site} must be on the order of 5×10^{-4} s (for $T_{IS} = T_{2C} \sim 10$ μs). This seems an unreasonably long correlation time given the likely local fluctuations in the macromolecular structure and/or local motions of the solvent molecules in the dipolar-coupled site.

In the present work, the interpretation of the magnitude of the dipolar coupling, κ_{dip}, is based on the relative motions of the hydrogens in the coupling site being more mobile than in the macromolecular matrix and therefore the magnitude of κ_{dip} will be smaller than $1/T_{2C}$. Also, it is found that if κ_{dip} is larger than about 100 s^{-1}, it is not possible to model empirical MT data as a function of temperature with the theoretical model presented here.

Dependence of MT on Hydrogen Populations

Magnetization transfer spectra as a function of f_{CA} and n_B as given in Table 1 are presented in Fig. 3. The number of dipolar-coupled solvent hydrogens, n_B, will decrease with fewer binding

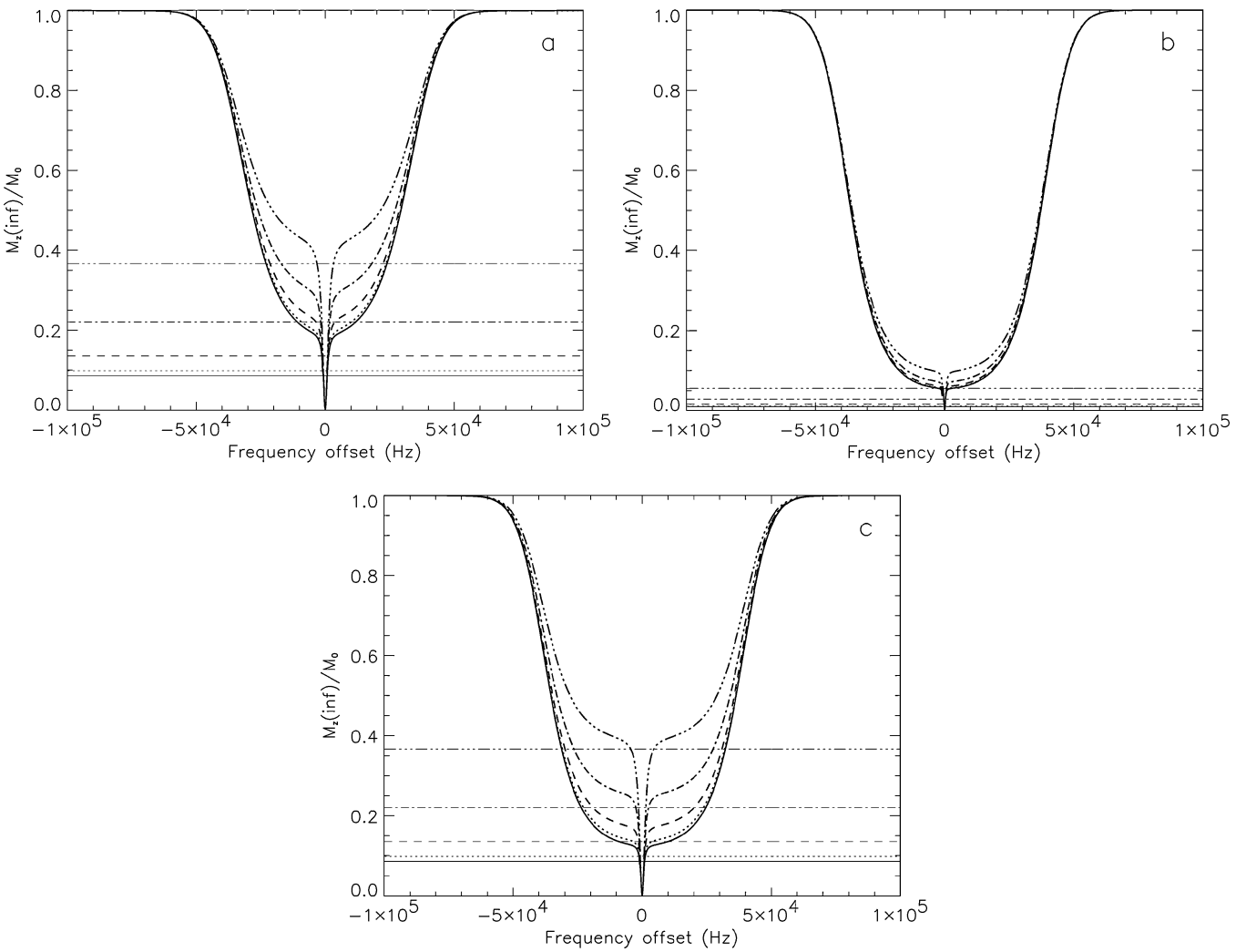

FIG. 3. Dependence of MT on relative hydrogen populations, Eq. [7, 8]. (a) MT spectra as a function of the number of solvent hydrogens bound in the dipolar coupling site, n_B. n_B decreases as a function of temperature due to a weak binding constant, K_b; see Table 1b. (—) 273 K; (· · ·) 298 K; (– – –) 323 K; (–·–) 348 K; (–· · ·–) 373 K. All other parameters are held constant to observe only the effect of n_B. R_{1A}: 1.0 s^{-1}, T_{2A}: 0.06 s, κ_{ex}: 1000 s^{-1}, R_{1B}: 2.0 s^{-1}, T_{2B}: 0.002 s, κ_{dip}: 15 s^{-1}, R_{1C}: 5.0 s^{-1}, σ_C: 15,000 Hz. The corresponding horizontal lines are the maximum magnetization transfer effect under conditions of complete saturation of the macromolecular magnetization, Eq. [16]. (b) MT spectra as a function of n_B with an increase in the concentration of macromolecules, $[S_{tot}] = 0.01$ M. The ratio of macromolecular hydrogens to bulk-solvent hydrogens increases by a factor of 10, $f_{CA} = 0.75$, and the ratio of bound to bulk-solvent hydrogens, f_{BA}, decreases by a factor of 10. n_B remains the same as in Table 1b. All other relaxation parameters are the same as in (a). (c) MT spectra as a function of n_B under conditions where the solvent water has been diluted by a factor of 10 with D_2O, Table 1c. All other relaxation parameters are the same as for (a).

sites, fewer hydrogens per bound solvent molecule, and/or weak solvent–macromolecular binding constants. The dependence of the bulk-solvent signal intensity on n_B enters through the intermolecular dipolar coupling $f_{CA}\kappa_{dip}^{CB} = f_{CA}n_B\kappa_{dip}$. For a given concentration of macromolecules, the effect of a smaller n_B will be to decrease κ_{dip}^{CB}. f_{CA} will remain nearly constant when the B-pool is small. The example shown in Fig. 3a demonstrates the resulting decrease in the magnetization transfer effect when n_B decreases as a function of temperature as a result of a weak binding constant, K_b.

An increase in the concentration of macromolecules results in an increase in f_{CA}. The degree of magnetization transfer will increase (Fig. 3b) as f_{CA} becomes larger as a result of an increase in κ^{AC} (Eq. [14]), as well as an increase in the relative contribution of the macromolecular relaxation, as most easily seen in Eq. [15]. n_B, and therefore κ_{dip}^{CB}, will not change with the concentration of macromolecules.

The effects of isotopic dilution will be apparent in both n_B and f_{CA}. n_B will decrease by the dilution factor and f_{CA} will increase by the same factor, and therefore there will be a small dependence of κ^{AC} on dilution, especially under the conditions of rapid exchange. As with an increase in macromolecular concentration, the effect of the increase in f_{CA} with dilution will be to increase the relative contribution of the macromolecular relaxation parameters to the MT spectrum; see Eq. [5], and compare Figs. 3a and 3c.

Dependence of MT on κ_{dip} and κ_{ex}

The magnitude of MT becomes independent of κ_{dip}^{CB} and κ_{ex}^{AB} as these rate constants get large; see Eq. [15]. The condition which must be met is

$$\frac{\kappa^{AC}}{f_{CA}} \gg R_{1C}, R_{RFC}$$

or

$$\frac{\kappa_{ex}^{AB}\kappa_{dip}^{CB}}{f_{BC}R_B}\left(\frac{f_{BC}}{f_{BA}}\right) \approx \frac{\kappa_{ex}^{AB}\kappa_{dip}^{CB}}{\kappa_{ex}^{AB} + f_{CA}\kappa_{dip}^{CB}} \gg R_{1C}, R_{RFC}. \quad [25]$$

R_{1C} will be on the order of 10 s^{-1}, and under standard experimental conditions where $\omega_1 \sim 3000$ rad s^{-1} and $\sigma_C \sim 20{,}000$ Hz, $R_{RFC} < 1$. Magnetization transfer spectra as a function of the coupling constants κ_{dip}^{CB} and κ_{ex}^{AB} are presented in Fig. 4. Figure 4 is a plot of the magnitude of magnetization transfer, $M_z^A(\infty)/M_0^A$, at $\Delta_A = 10$ kHz as calculated using Eq. [A1] as a function of κ_{dip}^{CB} and κ_{ex}^{AB} with all other parameters held constant. It is apparent from these plots that the condition in Eq. [25] is met when κ_{ex}^{AB} and κ_{dip} are greater than about 50 s^{-1}. This means that when attempting to fit magnetization transfer data, reliable values for the dipolar-coupling and exchange rates will not be able to be extracted with confidence when these rates exceed this limit.

MT Spectra as a Function of Temperature: Limiting Parameters and Modeling Trends in Empirical Data

The temperature dependence of the magnetization transfer spectrum must reflect the characteristic temperature dependence of the processes and system parameters which are limiting the degree of detectable coupling between the macromolecular and bulk-solvent populations. The temperature-dependent processes and parameters on which $M_z^A(\infty)/M_0^A$ will depend are the spin–lattice and spin–spin relaxation of the bulk and macromolecular hydrogen populations, the ratio of macromolecular to bulk hydrogens f_{CA}, the number of bound solvent hydrogens n_B, the strength of the dipolar coupling κ_{dip}, and the hydrogen physical exchange rate between the intermediate and bulk-solvent populations κ_{ex}^{AB}. The predominant effects of these factors on the magnetization transfer are considered below.

Spin–lattice relaxation in the bulk phase will affect how long-lived the dipolar transfer will be in the bulk-solvent phase. As the temperature increases, T_{1A} will increase since it scales with the reciprocal of the correlation time describing motions in the bulk solvent. Longer T_{1A} values will essentially increase the observed magnetization transfer effect because there is more time for the dipolar saturation transfer effect to build up in the bulk-solvent phase. Spin–lattice relaxation in the macromolecular phase will effect the efficiency of saturation. If T_{1C}, does change with temperature, the longer T_{1C}, the more efficient the saturation, and the greater the observable magnetization transfer effect. The predominant effect of T_{2A} and T_{2C} will be on the width of the direct and indirect saturation effect. Both scale inversely with the appropriate correlation times and therefore will get longer with increasing temperature. The width of the direct saturation "peak" (near $\Delta \sim 0$ Hz) and the indirect saturation in the MT spectrum will get narrower.

The strength of dipolar coupling, κ_{dip}, will depend on the dynamics of the coupling site. κ_{dip} will decrease with increasing temperature if τ_{site} gets shorter, contributing to a decrease in the observable magnetization transfer effect. κ_{dip} may also change with structural or conformational changes in the coupling site as a result of pH, solvent effects, and temperature, which may increase or decrease the separation between the coupled hydrogens. Physical exchange, κ_{ex}^{AB}, will increase with temperature and will contribute to an increase in the observed magnetization transfer effect if in the slow exchange limit, <50 s^{-1}. These slow exchange rates seem unlikely.

The temperature dependence of water–macromolecular magnetization transfer has been previously investigated in cross-linked bovine serum albumin (BSA) and heat-denatured ovalbumin (Fig. 5) (*28*, *42*). MT in BSA as a function of temperature has also been studied using other protonated solvents (*28*). The degree of MT and the dependence on temperature are characteristic of the system demonstrating the sensitivity of MT to solvent–macromolecular interactions.

To set up a comparable system to the BSA work presented by Hinton and Bryant, MT spectra were acquired on a sample of

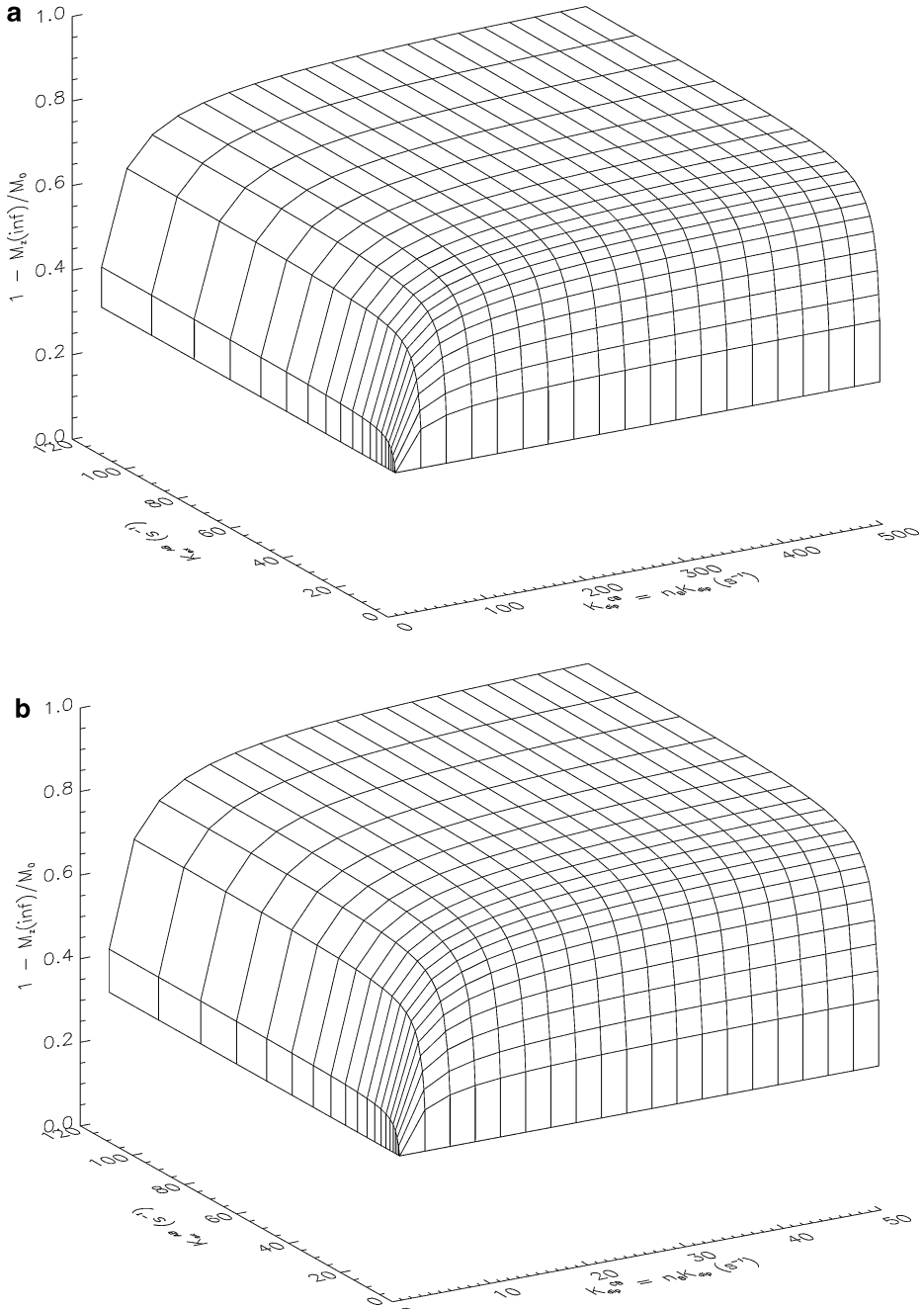

FIG. 4. The amplitude of the steady-state bulk-solvent magnetization enhancement, $1 - M_z^A(\infty)/M_0^A$, at $\Delta = 10{,}000$ Hz as a function of κ_{ex}^{AB} and κ_{dip}^{CB}. κ_{ex}^{AB} varies between 1.0 and 113 s^{-1}. κ_{dip} varies from 1.0 to 50 s^{-1}. (a) n_B equals 10. κ_{dip}^{CB} then varies from 10.0 to 500 s^{-1}. All other parameters are held constant: f_{BA}, 1.25×10^{-4}; f_{BC}, 1.67×10^{-3}; f_{CA}, 0.075; R_{1A}, 1.0 s^{-1}; T_{2A}, 0.02 s; R_{1B}, 2.0 s^{-1}; T_{2B}, 0.002 s; R_{1C}, 5.0 s^{-1}; σ_C, 15,000 Hz. (b) Same as in (a) except the bulk solvent has been diluted by a factor of 10. $n_B = 1.0$ and κ_{dip}^{CB} ranges from 1.0 to 50 s^{-1}.

hydrated cross-linked BSA. The sample was prepared following the procedure in Ref. (*28*). Magnetization transfer spectra are presented in Fig. 5a. The degree of magnetization transfer increases as a function of temperature. The MT spectrum linewidth is independent of temperature, which suggests that the gross dynamics of the macromolecular matrix are insensitive to temperature in this range and that it is reasonable to approximate that T_{2C} or σ_C are temperature independent (*34*). The temperature dependence of T_{1C} and κ_{dip} will depend on local motions within the macromolecular matrix and in the coupling site. T_{1C} will be assumed to be temperature independent as an initial approximation. It is consistent with the observed

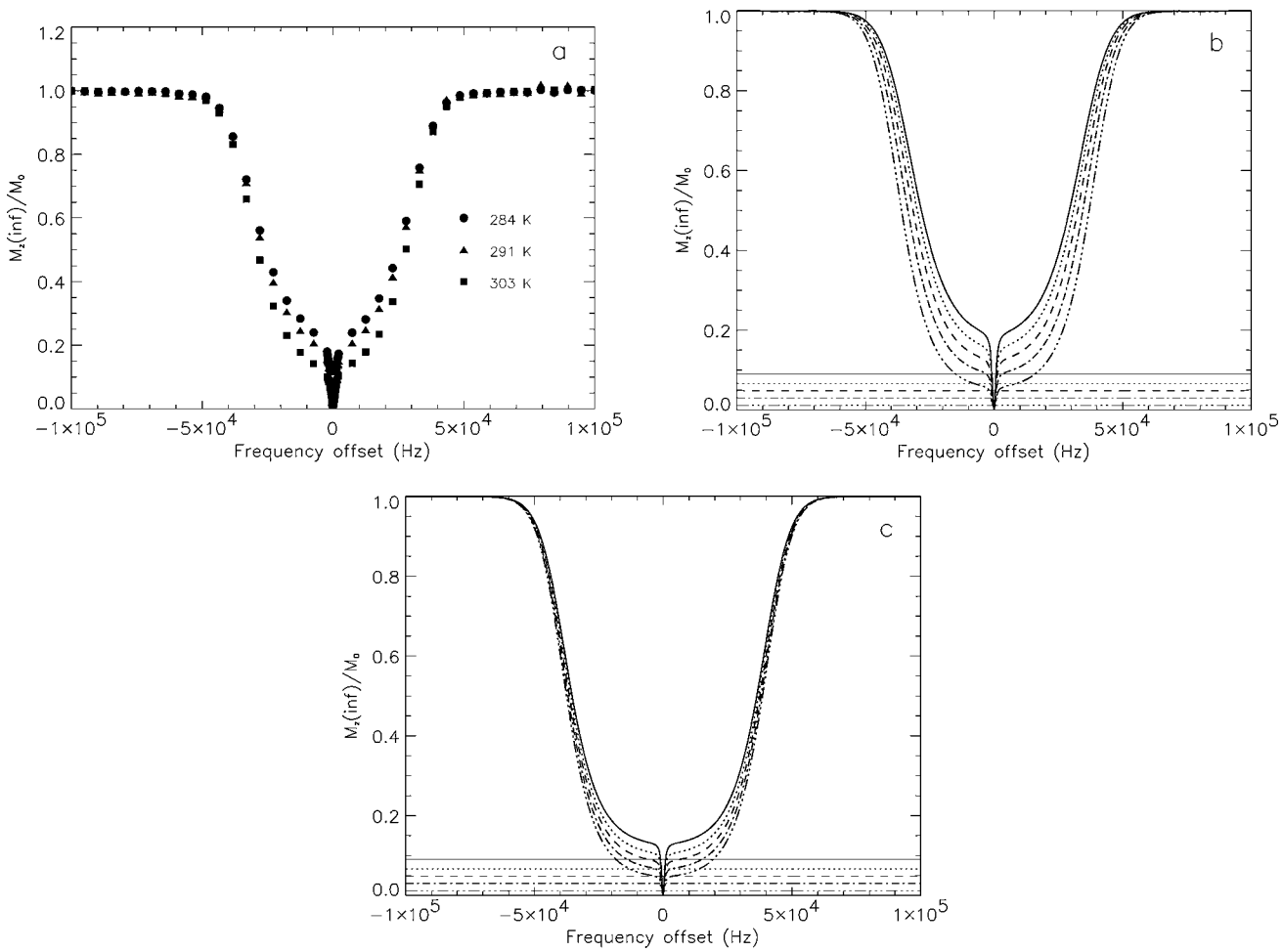

FIG. 5. Magnetization transfer in hydrated cross-linked bovine serum albumin. The sample was prepared following the procedure in Ref. (*28*). A total of 0.11 g of BSA (96–98% bovine albumin, Sigma Chemical Company) was dissolved in 0.91 g of H_2O. A 200 molar excess of glutaraldehyde was added to the BSA solution as 0.11 mL of a 25% aqueous solution of the cross-linking agent (25% aqueous solution, Grade II, Sigma Chemical Company). Magnetization transfer spectra as a function of temperature were acquired on a Bruker ARX300 spectrometer. (a) Experimental MT spectra acquired on a Bruker ARX300 spectrometer: (b) MT spectra calculated using Eqs. [7, 8]. f_{BA}, f_{BC}, f_{CA}, and n_B are given in Table 1a. (—) 273 K; (· · ·) 298 K; (– – –) 323 K; (–·–) 348 K; (–· · ·–) 373 K. The remaining relaxation parameters are listed in Table 3a. The corresponding horizontal lines are the maximum magnetization transfer effect under conditions of complete saturation of the macromolecular magnetization, Eq. [**16**]. (c) MT spectra calculated using Eqs. [7, 8] under conditions where the solvent, H_2O, has been diluted by a factor of 10 with the deuterated analog, D_2O. Parameters are given in Table 3a.

increase in the degree of magnetization transfer to also assume that κ_{dip} (and therefore τ_{site}) is insensitive to temperature in this range.

To model the albumin MT data, reasonable values for f_{CA} and n_B as a function of temperature were calculated assuming five binding sites per protein (*14, 28*), a binding equilibrium constant of 1.0, and a binding enthalpy appropriate for hydrogen bonding; see Table 1a. No temperature dependence is observed in these parameters. T_{1obs} increased from 1.5 to 2.6 s and T_{2obs} is approximately 60 ms. These are the short limits to T_{1A} and T_{2A}. Given the values and approximations for T_{1obs}, T_{2obs}, and f_{CA}, and assuming a low-temperature value for κ_{ex}^{AB} of 100 s^{-1}, the magnitude of $\kappa_{dip} = 15$ s^{-1} was chosen to approximate the observed depth of the MT spectrum. The increase in the observed magnetization transfer with temperature can thus be accounted for with the model presented here by increases in T_{1A}; see Fig. 5b. It is of note that the magnitude and behavior with temperature of the MT results for this sample of BSA match closely the results obtained for heat-denatured ovalbumin (*42*).

MT studies using bovine serum albumin are presented in the literature for samples approximately 10% by mass protein and a mixed solvent system approximately 10% by mass H_2O, 10–20% by mass other protonated polar solvents, and the remainder D_2O (*28*). As with ovalbumin and BSA in pure H_2O, an increase in water–protein magnetization transfer with temperature is observed. There is about a twofold increase in the magnitude of the magnetization transfer effect $(M_z^A(\infty)/M_0^A$ at $\Delta_A = 10$ kHz for BSA in H_2O ranges from 0.25 to 0.1, for BSA in the mixed

TABLE 2
f_{BA}, f_{BC}, and f_{CA} as a Function of Temperature

Temperature	K_b^c	$[L_{bound}]$	n_D	f_{DE}	f_{DC}	f_{CE}
		Acetone $[L_{tot}] = 2$ M				
		$n = 3$ $[S_{tot}] = 1 \times 10^{-3}$ M				
		$\Delta H_b = -20$ kJ dilution factor = 1.0				
273	0.0100	7.79×10^{-5}	0.47	3.90×10^{-5}	77.79×10^{-5}	0.50
298	0.00478	3.77×10^{-5}	0.23	1.89×10^{-5}	3.77×10^{-5}	0.50
323	0.00256	2.03×10^{-5}	0.12	1.02×10^{-5}	2.03×10^{-5}	0.50
348	0.00150	1.19×10^{-5}	0.072	5.96×10^{-5}	1.19×10^{-5}	0.50
373	0.000942	7.52×10^{-6}	0.045	3.76×10^{-5}	7.52×10^{-5}	0.50
		Methanol $[L_{tot}] = 3M$				
		$n = 2$ $[S_{tot}] = 1 \times 10^{-3}$ M				
		$\Delta H_b = -20$ kJ dilution factor = 1.0				
Temperature	K_b^c	$[L_{bound}]$	n_F	f_{FG}	f_{FC}	f_{CG}
273	0.0100	8.61×10^{-5}	0.34	2.87×10^{-5}	5.74×10^{-5}	0.50
298	0.00478	4.21×10^{-5}	0.17	1.40×10^{-5}	2.81×10^{-5}	0.50
323	0.00256	2.27×10^{-5}	0.091	7.58×10^{-6}	1.52×10^{-5}	0.50
348	0.00150	1.34×10^{-5}	0.053	4.46×10^{-6}	8.92×10^{-6}	0.50
373	0.000942	8.44×10^{-6}	0.034	2.81×10^{-6}	5.63×10^{-6}	0.50

Note. The data presented are for a system in which the protein concentration is 1×10^{-3} M in a mixed solvent system of acetone, methanol, and water. $N_H^L = 6$ for acetone, $N_H^L = 4$ for methanol, $N_H^S = 6000$. D and F represent acetone hydrogens and methanol hydrogens, respectively, bound in dipolar coupling sites.

TABLE 3
Relaxation Parameters Used in the Calculation of Magnetization Transfer Spectra Presented in Figs. 2, 5, and 6

Temperature	R_{1A} (s^{-1})	R_{1B} (s^{-1})	R_{1C} (s^{-1})	T_{2A} (s)	T_{2B} (s)	σ_C (Hz)	κ_{ex}^{AB} (s^{-1})	κ_{dip} (s^{-1})
273 K	1	2	5	0.06	0.002	15,000	100	15
298 K	0.78	1.8	5	0.06	0.0028	15,000	440	15
323 K	0.57	1.5	5	0.06	0.0035	15,000	1530	15
348 K	0.35	1.3	5	0.06	0.0043	15,000	4460	15
373 K	0.13	1	5	0.06	0.005	15,000	11,300	15

Temperature	R_{1A} (s^{-1})	R_{1C} (s^{-1})	T_{2A} (s)	σ_C (Hz)	κ_{ex}^{AB} (s^{-1})	κ_{dip} (s^{-1})
273 K	0.5	5	0.06	15,000	100	15
298 K	0.43	5	0.06	15,000	440	15
323 K	0.35	5	0.06	15,000	1530	15
348 K	0.28	5	0.06	15,000	4460	15
373 K	0.2	5	0.06	15,000	11,300	15

Temperature	R_{1E} (s^{-1})	R_{1C} (s^{-1})	T_{2E} (s)	σ_C (Hz)	κ_{ex}^{ED} (s^{-1})	κ_{dip} (s^{-1})
273 K	1	5	0.06	15,000	1000	10
298 K	0.88	5	0.06	15,000	2100	10
323 K	0.75	5	0.06	15,000	3900	10
348 K	0.63	5	0.06	15,000	6700	10
373 K	0.5	5	0.06	15,000	10,600	10

Temperature	R_{1G} (s^{-1})	R_{1C} (s^{-1})	T_{2G} (s)	σ_C (Hz)	κ_{ex}^{GF} (s^{-1})	κ_{dip} (s^{-1})
273 K	1.1	5	0.06	15,000	1000	5
298 K	0.98	5	0.06	15,000	2100	5
323 K	0.85	5	0.06	15,000	3900	5
348 K	0.73	5	0.06	15,000	6700	5
373 K	0.6	5	0.06	15,000	10,600	5

solvent system $M_z^A(\infty)/M_0^A$ at $\Delta_A = 10$ kHz ranges from 0.13 to 0.05). The relative increase in the water magnetization transfer for the BSA sample in the mixed solvent system with respect to the BSA samples in H_2O can be accounted for by the effects of dilution of the water with D_2O; see Fig. 5c. Isotopic dilution leads to increases in the observable MT due to an increase in f_{CA} and relative contributions of the macromolecular relaxation parameters; see Fig. 3. An increase in T_{1A} due to decreased inter- and intramolecular proton–proton interactions in the diluted solvent may also lead to a relative increase in the observable magnetization transfer effect. Hinton and Bryant argue that the behavior of the magnetization transfer with temperature is attributable to competing effects of whole-solvent exchange and exchange of labile hydrogens. Labile hydrogen exchange is treated as a separate pathway for magnetization transfer which does not include dipolar transfer. The authors then argue that the increase in water–macromolecular magnetization transfer with temperature is a result of the increase in exchange rate with temperature. Previous results have demonstrated that hydrogen exchange alone is not a sufficient mechanism to account for magnetization transfer (*17*). Consistent with the model presented here, the increase in magnetization transfer may be accounted for by the increase in T_{1A} with temperature.

The model and parameter constraints presented here are easily extended to interpret experimental magnetization transfer in the water/acetone/methanol tertiary solvent system used by Bryant and Hinton. In contrast to what is observed for water, a decrease in magnetization transfer was observed with temperature for both acetone and methanol (*28*). Also, a significant decrease in the magnitude of solvent–macromolecular magnetization transfer was observed for both acetone and methanol compared to water. The latter effect may be accounted for by weaker dipolar coupling as a result of a larger solvent–macromolecular intermolecular spacing as a result of acetone and methanol being both larger than water and less tightly held at the macromolecular surface due to weaker intermolecular binding. With respect to the model and constraints presented here, the intermolecular dipolar coupling, κ_{dip}^{CB}, is the only parameter which can lead to a decrease in MT with increasing temperature. If the argument is made as above for the water–macromolecular MT, that κ_{dip} is insensitive to temperature, then the same must hold for magnetization transfer associated with the other solvents. For κ_{dip}^{CB} to decrease, then n_B must decrease, which necessitates a weak binding constant for these solvents; see Table 2. This is consistent with the arguments presented by Hinton and Bryant.

Using a parallel model for the solvent–macromolecular couplings and using the two-pool approximation for each solvent–macromolecular coupling, the steady-state coupled rate equations for a tertiary solvent system are given by

$$-R_{1A} = -\left(R_{1A} + \kappa_{eff}^{AC} + R_{RFA}\right)\frac{M_z^A(\infty)}{M_0^A} + \kappa_{eff}^{AC}\frac{M_z^C(\infty)}{M_0^C}$$

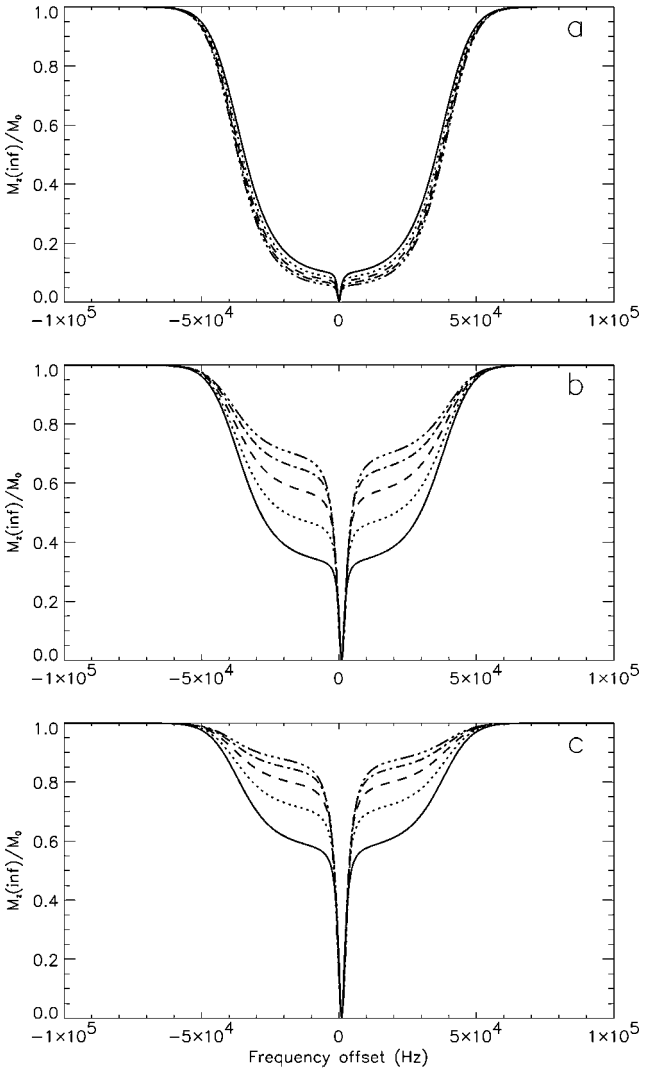

FIG. 6. Magnetization transfer spectra calculated using Eq. [26] modeling cross-linked bovine serum albumin in a mixed solvent system. (a) Solvent–BSA magnetization transfer based on f_{BA}, f_{BC}, f_{CA}, and n_B calculated using the parameters for Table 1a except for a dilution factor of 0.1 modeling the water MT. The remaining relaxation parameters are listed in Table 3b. (b) Solvent–BSA magnetization transfer based on f_{DE}, f_{DC}, f_{CE}, and n_D data presented in Table 2a modeling the acetone MT. The remaining relaxation parameters are listed in Table 3c. (c) Solvent–BSA magnetization transfer based on f_{FG}, f_{FC}, f_{CG}, and n_F data in Table 2b modeling the methanol MT. The remaining relaxation parameters are listed in Table 3d.

$$-R_{1E} = -\left(R_{1E} + \kappa_{eff}^{EC} + R_{RFE}\right)\frac{M_z^E(\infty)}{M_0^E} + \kappa_{eff}^{EC}\frac{M_z^C(\infty)}{M_0^C}$$

$$-R_{1G} = -\left(R_{1G} + \kappa_{eff}^{GC} + R_{RFG}\right)\frac{M_z^G(\infty)}{M_0^G} + \kappa_{eff}^{GC}\frac{M_z^C(\infty)}{M_0^C}$$

$$-R_{1C} = -\left(R_{1C} + \frac{\kappa_{eff}^{AC}}{f_{CA}} + \frac{\kappa_{eff}^{EC}}{f_{CE}} + \frac{\kappa_{eff}^{GC}}{f_{CG}} + R_{RFC}\right)\frac{M_z^C(\infty)}{M_0^C} + \frac{\kappa_{eff}^{AC}}{f_{CA}}\frac{M_z^A(\infty)}{M_0^A} + \frac{\kappa_{eff}^{EC}}{f_{CE}}\frac{M_z^E(\infty)}{M_0^E} + \frac{\kappa_{eff}^{GC}}{f_{CG}}\frac{M_z^G(\infty)}{M_0^G}, \quad [26]$$

where E represents bulk-solvent acetone and G represents bulk-solvent methanol. The effective coupling constants, κ_{eff}^{XC}, are given by Eqs. [9, 14] with the appropriate substitutions for the respective solvents. Solving these equations for $M_z^{\text{A}}(\infty)/M_0^{\text{A}}$, $M_z^{\text{E}}(\infty)/M_0^{\text{E}}$, and $M_z^{\text{G}}(\infty)/M_0^{\text{G}}$ using the data in Tables 2 and 3 gives the magnetization transfer spectra presented in Fig. 6 which are consistent with the trends observed for the acetone– and methanol–BSA magnetization transfer (*28*).

CONCLUSIONS

A three-pool model is presented and used to model solvent–macromolecular hydrogen magnetization transfer, explicitly including the population of solvent hydrogens which are coupled by through-space dipolar exchange with the macromolecular hydrogens and by physical exchange with the bulk-solvent hydrogens. In most biological systems, the fraction of this population of hydrogens is small. Under these conditions, the steady-state bulk-solvent magnetization is independent of the relaxation parameters of these surface hydrogens. This leads to the argument that the three-pool model is well-approximated by a two-pool model for the coupling between the bulk-solvent and macromolecular hydrogens. When a two-pool model is used, the coupling constant must be defined to include both the physical exchange and the dipolar magnetization transfer rates combined to reflect a series coupled system. The dipolar coupling is intermolecular and is described by the pseudo-first-order rate constant, $\kappa_{\text{dip}}^{\text{CB}} = n_{\text{B}}\kappa_{\text{dip}}$, which contains an explicit dependence on the number of dipolar-coupled solvent hydrogens.

Because of the number of parameters on which the equilibrium bulk-solvent signal intensity depends, it is difficult to extract a unique and meaningful set of values which will describe a magnetization transfer spectrum or set of spectra. However, by constraining the search for parameter values to physically meaningful ranges based on the relevant conditions of the system and on observed trends in empirical magnetization transfer, more meaningful results can be obtained which improve the interpretation of magnetization transfer spectra as well as the predictive power of the model. An important finding is that the degree of magnetization transfer becomes independent of the physical exchange rate, $\kappa_{\text{ex}}^{\text{AB}}$, and the intrinsic dipolar transfer rate, κ_{dip}, when these parameters are greater than about 50 to 100 s^{-1}. Using the three-pool model and a set of constrained parameters, the analysis of magnetization transfer in systems where the supramolecular structure is insensitive to temperature showed that the magnetization transfer is primarily limited by the intermolecular dipolar transfer, $\kappa_{\text{dip}}^{\text{CB}}$, and the spin–lattice relaxation in the bulk phase, $T_{1\text{A}}$. In systems such as less rigid bilayer structures and tissues pathologies where the dynamics and/or extent of the macromolecular matrix are sensitive to sample conditions, the degree of magnetization transfer may also be sensitive to changes in the relaxation parameters of the macromolecular hydrogens, $T_{1\text{C}}$ and σ_{C}.

The description presented here for the relationship between the observable bulk-solvent magnetization transfer effect and the physicochemistry of the solvated macromolecular system incorporates many of the ideas which have been presented in the literature and leads to a quantitative model which predicts the trends observed in experimental data using a relevant set of parameters. These sets of parameters could be used as initial input estimates to a more complete analytical analysis of MT data. This rational and constrained approach to the interpretation of magnetization transfer data is critical for extracting reliable information about complex and *in vivo* systems. The interpretation of the mechanism for magnetization transfer and parameter constraints contributes to furthering our understanding of and enhances the ability to interpret MRI and MT contrast and changes in contrast in terms of chemical, structural, and dynamic factors associated with tissue pathology. In a more general sense, the model enhances the usefulness of water NMR as a probe of physicochemical properties of hydrated macromolecular systems.

APPENDIX A

The steady-state solutions to Eq. [1] for the longitudinal components are given by

$$
\begin{aligned}
-R_{1\text{A}} &= -\left(R_{1\text{A}} + \kappa_{\text{ex}}^{\text{AB}} + \frac{\omega_1^2}{F1}\right)\frac{M_z^{\text{A}}(\infty)}{M_0^{\text{A}}} \\
&\quad + \left(\kappa_{\text{ex}}^{\text{AB}} + f_{\text{BA}}\left(\frac{\omega_1^2 E1}{F1E4}\right)\right)\frac{M_z^{\text{B}}(\infty)}{M_0^{\text{B}}} \\
-R_{1\text{B}} &= -\left(R_{1\text{B}} + \frac{\kappa_{\text{ex}}^{\text{AB}}}{f_{\text{BA}}} + \frac{\kappa_{\text{dip}}^{\text{CB}}}{f_{\text{BC}}} + \frac{\omega_1^2}{F2}\right)\frac{M_z^{\text{B}}(\infty)}{M_0^{\text{B}}} \\
&\quad + \frac{1}{f_{\text{BA}}}\left(\kappa_{\text{ex}}^{\text{AB}} + \left(\frac{\omega_1^2 E3}{F2E2}\right)\right)\frac{M_z^{\text{A}}(\infty)}{M_0^{\text{A}}} + \frac{\kappa_{\text{dip}}^{\text{CB}}}{f_{\text{BC}}}\frac{M_z^{\text{C}}(\infty)}{M_0^{\text{C}}} \\
-R_{1\text{C}} &= -\left(R_{1\text{C}} + \kappa_{\text{dip}}^{\text{CB}} + R_{\text{RFC}}\right)\frac{M_z^{\text{C}}(\infty)}{M_0^{\text{C}}} + \kappa_{\text{dip}}^{\text{CB}}\frac{M_z^{\text{B}}(\infty)}{M_0^{\text{B}}},
\end{aligned}
\qquad \text{[A1]}
$$

with the following definitions and conditions,

$$
M_0^{\text{A}}\kappa_{\text{ex}}^{\text{AB}} = M_0^{\text{B}}\kappa_{\text{ex}}^{\text{BA}}, \quad \frac{M_0^{\text{B}}}{M_0^{\text{A}}} = f_{\text{BA}}
$$

$$
M_0^{\text{B}}\kappa_{\text{dip}}^{\text{BC}} = M_0^{\text{C}}\kappa_{\text{dip}}^{\text{CB}}, \quad \frac{M_0^{\text{B}}}{M_0^{\text{C}}} = f_{\text{BC}}
$$

$$
R_{2\text{A}} = \frac{1}{T_{2\text{A}}} + \kappa_{\text{ex}}^{\text{AB}}, \quad R_{2\text{B}} = \frac{1}{T_{2\text{B}}} + \frac{\kappa_{\text{ex}}^{\text{AB}}}{f_{\text{BA}}},
$$

$$
D1 = R_{2\text{B}} - \frac{\left(\kappa_{\text{ex}}^{\text{AB}}\right)^2}{f_{\text{BA}}R_{2\text{A}}}, \quad D2 = R_{2\text{A}} - \frac{\left(\kappa_{\text{ex}}^{\text{AB}}\right)^2}{f_{\text{BA}}R_{2\text{B}}},
$$

$$E1 = \frac{\kappa_{ex}^{AB}}{f_{BA}}\left(1-\left(\frac{4\pi^2\Delta_A\Delta_B}{R_{2B}D2}\right)\right), \quad E2 = R_{2A} + \frac{4\pi^2\Delta_A^2}{D2},$$

$$E3 = \kappa_{ex}^{AB}\left(1-\left(\frac{4\pi^2\Delta_A\Delta_B}{R_{2A}D1}\right)\right), \quad E4 = R_{2B} + \frac{4\pi^2\Delta_B^2}{D1},$$

$$F1 = \frac{E1\times E3}{E4} - E2, \quad F2 = \frac{E3\times E1}{E2} - E4. \qquad [A2]$$

ACKNOWLEDGMENTS

Acknowledgment is made to the donors of The Petroleum Research Fund, administered by the ACS, for partial support of this research. The authors gratefully acknowledge the support of the Departments of Chemistry and Chemical Engineering at Bucknell University. We thank Dr. Marty Ligare for helpful discussions concerning intermolecular dipolar magnetization exchange and our students, Michael Moore and Dan Livingston, for their contributions to this work. We appreciate the thoughtful and helpful comments of the reviewers.

REFERENCES

1. F. Svec and J. M. J. Fréchet, New designs of macroporous polymers and supports: From separation to biocatalysis, *Science* **273,** 205–211 (1996).
2. R. Dagani, Intelligent gels, *Chem. Eng. News* **June 9,** 26–37 (1997).
3. R. E. Fornes and R. D. Gilbert, Environmental effects of polymers, *Polym. Fiber Sci. Recent Adv.* **1992,** 1.
4. L. Banks and B. Ellis, The glass transition temperature of an epoxy resin and the effect of absorbed water, *Polymer Bull.* **1,** 377 (1979).
5. R. P. Kennan, K. A. Richardson, J. Zhong, M. J. Maryanski, and J. C. Gore, The effects of cross-link density and chemical exchange on magnetization transfer in polyacrylamide gels, *J. Magn. Reson. B* **110,** 267–277 (1996).
6. J. J. Tessier, K. Potter, T. A. Carpenter, and L. D. Hall, Demonstration of the linear dependence of proton magnetization transfer on polymer concentration in aqueous gels at two different field strengths, *Magn. Reson. Chem.* **32,** 55–61 (1994).
7. K. Overloop and L. Van Gerven, Exchange and cross-relaxation in adsorbed water, *J. Magn. Reson. A* **101,** 147–156 (1993).
8. M. Whaley, A. J. Lawrence, J.-P. Korb, and R. G. Bryant, Magnetic cross-relaxation and chemical exchange between microporous solid and mobile liquid phases, *Solid State Nucl. Magn. Reson.* **7,** 247–252 (1996).
9. R. M. Brunne, E. Liepinsh, G. Otting, K. Wüthrich, and W. F. van Gunsteren, Hydration of proteins: A comparison of experimental residence times of water molecules solvating the bovine pancreatic trypsin inhibitor with theoretical model calculations, *J. Mol. Biol.* **231,** 1040–1048 (1993).
10. R. G. Bryant, The dynamics of water-protein interactions, *Annu. Rev. Biophys. Biomol. Struct.* **25,** 29–53 (1996).
11. A. M. Gottlied, P. T. Inglefield, and Y. Lange, Water–lecithin binding in lecithin–water lamellar phases at 20°C, *Biochim. Biophy. Acta* **307,** 444–451 (1973).
12. H. J. Berendsen, Nuclear magnetic resonance study of collagen hydration, *J. Chem. Phys.* **36,** 3297–3305 (1962).
13. R. Mathurs-De Vre, Biomedical implications of the relaxation behavior of water related to NMR imaging, *Br. J. Radiol.* **57,** 955 (1984).
14. S. H. Koenig, R. D. Brown III, and R. Ugolini, A unified view of relaxation in protein solutions and tissue, including hydration and magnetization transfer, *Magn. Reson. Med.* **29,** 77–83 (1993).
15. P. A. Bottomley, C. J. Hardy, R. E. Argersinger, and G. Allen-Moore, A review of ^{1}H nuclear magnetic resonance relaxation in pathology: Are T_1 and T_2 diagnostic?, *Med. Phys.* **14,** 1–36 (1987).
16. H. T. Edzes and E. T. Samulski, The measurement of cross-relaxation effects in the proton NMR spin–lattice relaxation of water in biological systems: Hydrated collagen and muscle, *J. Magn. Reson.* **31,** 207–229 (1978).
17. T. L. Ceckler and R. S. Balaban, Tritium–proton magnetization transfer as a probe of cross relaxation in aqueous lipid bilayer suspensions, *J. Magn. Reson.* **93,** 572–588 (1991).
18. G. Otting and E. Liepinsh, Protein hydration viewed by high-resolution NMR spectroscopy: Implications for magnetic resonance image contrast, *Acc. Chem. Res.* **28,** 171–177 (1995).
19. D. F. Gochberg, R. P. Kennan, M. J. Maryanski, and J. C. Gore, The role of specific side groups and pH in magnetization transfer in polymers, *J. Magn. Reson.* **131,** 191–198 (1998).
20. B. P. Hills, The proton exchange cross-relaxation model of water relaxation in biopolymer systems, *Mol. Phys.* **76,** 489–508 (1992).
21. I. Solomon, Relaxation processes in a system of two spins, *Phys. Rev.* **99,** 559–565 (1955).
22. S. H. Koenig, R. G. Bryant, K. Hallenga, and G. S. Jacob, Magnetic cross-relaxation among protons in protein solutions, *Biochemistry* **17,** 4348–4358 (1978).
23. O. K. Daszkiewicz, J. W. Hennel, B. Lubas, and T. W. Szczepkowski, Proton magnetic relaxation and protein hydration, *Nature* **200,** 1006–1007 (1963).
24. J. R. Zimmerman and W. E. Brittin, Nuclear magnetic resonance studies in multiple phase systems: Lifetime of a water molecule in an adsorbing phase on silica gel, *J. Phys. Chem.* **61,** 1328–1333 (1957).
25. R. A. Hoffman and S. Forsén, Transient and steady-state overhauser experiments in the investigation of relaxation processes. Analogies between chemical exchange and relaxation, *J. Chem. Phys.* **45,** 2049–2060 (1966).
26. S. D. Wolff and R. S. Balaban, Magnetization transfer contrast (MTC) and tissue water proton relaxation *in vivo*, *Magn. Reson. Med.* **10,** 135–144 (1989).
27. T. L. Ceckler, S. D. Wolff, V. Yip, S. A. Simon, and R. S. Balaban, Dynamic and chemical factors affecting water proton relaxation by macromolecules, *J. Magn. Reson.* **98,** 637–645 (1992).
28. D. P. Hinton and R. G. Bryant, ^{1}H magnetic cross-relaxation between multiple solvent components and rotationally immobilized protein, *Magn. Reson. Med.* **35,** 497–505 (1996).
29. B. P. Hills and F. A. Favret, A comparative multinuclear relaxation study of protein–DMSO and protein–water interactions, *J. Magn. Reson. B* **103,** 142–151 (1994).
30. R. S. Balaban and T. L. Ceckler, Magnetization transfer contrast in magnetic resonance imaging, *Magn. Reson. Q.* **8,** 116–137 (1992).
31. R. G. Bryant, Magnetization transfer and cross-relaxation in tissue, *in* "Encyclopedia of Nuclear Magnetic Resonance" (David M. Grant and Robin K. Harris, Eds.), Wiley, New York, 1996.
32. R. Baudouin, Magnetization transfer contrast: Clinical applications, *in* "Encyclopedia of Nuclear Magnetic Resonance" (David M. Grant and Robin K. Harris, Eds.), Wiley, New York, 1996.
33. J. Grad and R. G. Bryant, Nuclear magnetic cross-relaxation spectroscopy, *J. Magn. Reson.* **90,** 1–8 (1990).
34. T. L. Ceckler and R. G. Balaban, Field dispersion in water–macromolecular proton magnetization transfer, *J. Magn. Reson. B* **105,** 242–248 (1994).
35. E. Liepinsh and G. Otting, Proton exchange rates from amino acid side chains—Implications for image contrast, *Magn. Reson. Med.* **35,** 30–42 (1996).
36. W. Kucharczyk, P. M. Macdonald, G. J. Stanisz, and R. M. Henkelman, Relaxivity and magnetization transfer of white matter lipids and MR imaging: importance of cerebrosides and pH, *Radiology* **192,** 521–529 (1994).
37. S. H. Koenig, R. D. Brown III, M. Spiller, and Lundblom, Relaxometry of brain: Why white matter is white in MRI, *Magn. Reson. Med.* **14,** 482 (1990).

38. G. H. Caines, T. Schleich, and J. M. Rydzewski, Incorporation of magnetization transfer into the formalism for rotating-frame spin–lattice proton NMR relaxation in the presence of an off-resonance-irradiation field, *J. Magn. Reson.* **95,** 558–566 (1991).

39. R. M. Henkelman, X. Huang, Q.-S. Xiang, G. J. Stanisz, S. D. Swanson, and M. J. Bronskill, Quantitative interpretation of magnetization transfer, *Magn. Reson. Med.* **29,** 759–766 (1993).

40. J. G. Li, S. J. Graham, and R. M. Henkelman, A flexible magnetization transfer line shape derived from tissue experimental data, *Magn. Reson. Med.* **37,** 866–871 (1997).

41. R. S. Adler, S. D. Swanson, and H. H. Yeung, A three-component model for magnetization transfer. Solution by projection-operator technique, and application to cartilage, *J. Magn. Reson. B* **110,** 1–8 (1996).

42. T. L. Ceckler, V. Yip, S. A. Simon, and R. S. Balaban, An evaluation of the rate limiting processes in water-macromolecular proton magnetization transfer, *in* Abstracts of the Society of Magnetic Resonance in Medicine, 12th Annual Meeting, p. 178, (1993); T. L. Ceckler, Chemical basis of water macromolecule magnetization exchange, Proceedings of "A Workshop on MTC," Hood College, 1993.

43. X. Wu and J. J. Listinsky, Effects of transverse cross relaxation on magnetization transfer, *J. Magn. Reson. B* **105,** 73–76 (1994).

44. K. Kuwata, D. Brooks, H. Yua, and T. Schleich, Relaxation formalism for rotating-frame spin–lattice proton NMR relaxation and magnetization transfer in the presence of an off-resonance irradiation field, *J. Magn. Reson. B* **104,** 11–25 (1994).

45. S. D. Swanson, *in* Abstracts of the Society of Magnetic Resonance in Medicine, 11th Annual Meeting, p. 255 (1992).

46. J. G. Li, S. J. Graham, and R. M. Henkelman, A flexible magnetization transfer line shape derived from tissue experimental data, *Magn. Reson. Med.* **37,** 866–871 (1997).

47. H. N. Yeung, R. S. Adler, and S. D. Swanson, Transient decay of longitudinal magnetization in heterogeneous spin systems under selective saturation. IV. Reformulation of the spin-bath-model equations by the Redfield–Provotorov theory, *J. Magn. Reson. A* **106,** 37–45 (1994).

48. H. M. McConnell, Reaction rates by nuclear magnetic resonance, *J. Chem. Phys.* **28,** 430–431 (1958).

49. S. Macura and R. R. Ernst, Elucidation of cross relaxation in liquids by two-dimensional N.M.R. spectroscopy, *Mol. Phys.* **41,** 95–117 (1980).

50. K. E. van Holde, W. C. Curtis, and P. S. Ho, "Principles of Physical Biochemistry," Prentice Hall, NJ, 1998.

51. A. Abragam, "Principles of Nuclear Magnetism," Oxford Univ. Press, New York, 1961.

52. A. Kalk and H. J. C. Berendsen, Proton magnetic relaxation and spin diffusion in proteins, *J. Magn. Reson.* **24,** 343–366 (1976).

53. M. F. Brown, Theory of spin–lattice relaxation in lipid bilayers and biological membranes. Dipolar relaxation, *J. Chem. Phys.* **80,** 2808–2831 (1984).

54. L. Coppola, R. Muzzalupa, and G. A. Ranieri, Temperature dependence of water self-diffusion in the gel phase of a potassium palmitate system, *J. Phys. II France* **6,** 657–666 (1996).

55. K. J. Packer, The dynamics of water in heterogeneous systems, *Phil. Trans. R. Soc. Lond. B* **278,** 59–87 (1977).

56. A. L. Lee, P. F. Flynn, and A. J. Wand, Comparison of ^{2}H and ^{13}C NMR relaxation techniques for the study of protein methyl group dynamics in solution, *J. Am. Chem. Soc.* **121,** 2891–2902 (1999).

57. Z.-y. Peng, V. Simplaceanu, I. L. Lowe, and C. Ho, Slow molecular motions in lipid bilayers, *Biophys. J.* **54,** 81–95 (1988).

58. T. Endo, T. Ueda, H. Yamada, and T. Imoto, *Biochemistry* **26,** 1838–1845 (1987).

59. E. Tüchsen and C. Woodward, Hydrogen kinetics of peptides amide protons at the bovine pancreatic trypsin inhibitor protein–solvent interface, *J. Mol. Biol.* **185,** 405–419 (1985).

60. G. D. Henry and B. D. Sykes, Saturation transfer of exchangeable protons in ^{1}H-decoupled ^{15}N INEPT spectra in water. Application to the measurement of hydrogen exchange rates in amides and proteins, *J. Magn. Reson. B* **102,** 193–200 (1993).

61. L. T. Kakalis and T. F. Kumosinski, The dynamics of water in protein solutions: The field dispersion of deuterium NMR longitudinal relaxation, *Biophys. Chem.* **43,** 39–49 (1992).

62. M. E. Rogers, J. J. Englander, S. W. Englander, and W. F. Harrington, *Biophys. Chem.* **59,** 221–230 (1996).

63. K. Venu, V. P. Denisov, and B. Halle, Water ^{1}H magnetic relaxation dispersion in protein solutions. A quantitative assessment of internal hydration, proton exchange, and cross-relaxation, *J. Am. Chem. Soc.* **119,** 3122–3134 (1997).

64. J. H. Noggle and R. E. Shirmer, "The Nuclear Overhauser Effect: Chemical Applications," Academic Press, New York, 1971.